Adult Neurogenesis Reconciles Flexibility and Stability of Olfactory Perceptual Memory

Bennet Sakelaris[a] **and Hermann Riecke**[a]

***For correspondence:**
bennetsakelaris@u.northwestern.edu (BS); h-riecke@northwestern.edu (HR)

[a]Engineering Sciences and Applied Mathematics, Northwestern University, Evanston, Illinois, United States of America

Abstract In brain regions featuring ongoing plasticity, the task of quickly encoding new information without overwriting old memories presents a significant challenge. In the rodent olfactory bulb, which is renowned for substantial structural plasticity driven by adult neurogenesis and persistent turnover of dendritic spines, we show that by synergistically combining both types of plasticity this flexibility-stability dilemma can be overcome. To do so, we develop a computational model for structural plasticity in the olfactory bulb and show that it is the maturation process of adult-born neurons that enables the bulb to learn quickly and forget slowly. Particularly important are the transient enhancement of the plasticity, excitability, and susceptibility to apoptosis that characterizes young neurons. The model captures many experimental observations and makes a number of testable predictions. Overall, it identifies memory consolidation as an important role of adult neurogenesis in olfaction and exemplifies how the brain can maintain stable memories despite ongoing extensive neurogenesis and synaptic plasticity.

Introduction

The learning and the subsequent retention of information are fundamental tasks of the brain. One crucial form of learning is perceptual learning where an animal learns to discriminate between similar stimuli through repeated experience. Importantly, perceptual learning is a form of continual learning and occurs even in the absence of explicit rewards or aversions that may modulate plasticity. Thus, in this situation the brain faces the "flexibility-stability dilemma" ***Grossberg*** (***1982***), wherein the acquisition of memories should be flexible enough to continually encode new memories but stable enough that new stimuli do not overwrite old memories.

The flexibility-stability dilemma can classically be resolved through the process of systems consolidation where memories are rapidly encoded by the hippocampus and gradually transferred to the neocortex where they remain quite stable ***McClelland et al.*** (***1995***); ***Roxin and Fusi*** (***2013***). In systems where consolidation is restricted to the very circuit that encoded the information in the first place, it is not yet well understood how this issue is combated. It has previously been addressed in models built on theoretical, complex synapses that are characterized by cascades of depressed and potentiated states ***Fusi et al.*** (***2005***); ***Benna and Fusi*** (***2016***); however, detailed experimental evidence for systems in which this local mechanism resolves this issue without making use of systems consolidation is not yet available.

Here, we address this issue by considering the olfactory system, where perceptual learning has been shown to occur in the olfactory bulb (OB) ***McNamara et al.*** (***2008***); ***Gschwend et al.*** (***2015***),

which is renowned for its high degree of structural plasticity, most notably through adult neurogenesis. Experiments have shown that adult neurogenesis is necessary for certain forms of perceptual learning ***Moreno et al.*** (***2009***); ***Li et al.*** (***2018***), and computational modeling provides some understanding of the underlying mechanisms ***Chow et al.*** (***2012***); ***Adams et al.*** (***2019***); ***Shani-Narkiss et al.*** (***2020***); ***Kersen et al.*** (***2022***). However, these behavioral observations could also be explained by synaptic plasticity alone ***Sailor et al.*** (***2016***); ***Meng and Riecke*** (***2022***). What, then, is the purpose of adding large numbers of new neurons? And why remove a sizable fraction of them again later?

Using a computational model of the OB, we demonstrate that the synergistic interaction between adult neurogenesis and synaptic plasticity can provide a massive computational advantage in olfactory memory by ameliorating the flexibility-stability dilemma. Importantly, it is not the adding of neurons as such but the maturation process of the adult-born neurons that achieves this goal: the experimentally observed heightened excitability and plasticity of newly arrived young cells ***Kelsch et al.*** (***2009***); ***Nissant et al.*** (***2009***); ***Wallace et al.*** (***2017***) allow them to rapidly store new memories when they are young; the memories then stabilize as the aging neurons become less plastic. Furthermore, the transiently increased excitability of new neurons is important for helping them integrate into the network, while on longer time scales, their higher rate of apoptosis is needed to remove unnecessary neurons that would interfere with the ability of newer neurons to integrate when learning new odors.

Our biophysically motivated model captures a host of recent experimental observations, including how adult-born neurons are preferentially recruited to process new odors ***Moreno et al.*** (***2009***); ***Forest et al.*** (***2019***, 2020), and how the silencing of these neurons extinguishes memory ***Forest et al.*** (***2020***). Additionally, young neurons are highly sensitive to retrograde interference and die if a new odor is presented without the previously presented odor still being present in the environment ***Forest et al.*** (***2019***). Moreover, our model makes multiple experimentally testable predictions including that the rapid re-learning of a forgotten odor pair ***Sultan et al.*** (***2010***) is enabled by the sensory-dependent dendritic elaboration of neurons that initially encoded the odors, and that the observed rapid re-learning would occur even if neurogenesis was blocked following the first enrichment and even though the initial learning did require neurogenesis. Furthermore, long time periods without odor enrichment or without apoptosis are predicted to negatively impact the subsequent ability to learn new odors.

Results

We studied the effects of adult neurogenesis in a structurally constrained computational model that was designed to include many important, specific biological aspects of the olfactory bulb. Previous theoretical work has found conflicting results regarding the effects of new neurons on old memories, and the findings seem to depend sensitively on the implementation of neurogenesis, network architecture, and task ***Aimone and Gage*** (***2011***). Although simpler models could be used to investigate adult neurogenesis, to gain biological insight it is therefore essential to study neurogenesis in a model derived from the relevant biological processes and tasks.

Formulation of the model

We considered an OB network comprising two distinct layers of neurons: the primary layer consisting of excitatory mitral cells (MCs) and the secondary layer composed of inhibitory granule cells (GCs), the preeminent neurogenic population in the OB. We omit preprocessing in the glomerular layer, although it also involves adult-neurogenesis, but on a much smaller scale ***Lledo et al.*** (***2006***). In each timestep, new adult-born granule cells (abGCs) were added to the GC layer. The MCs received sensory input via glomerular activation patterns, forming representations of the stimuli in terms of the MC activity. These representations were reformatted by the inhibition provided by the reciprocal connections between MCs and GCs and were projected to the olfactory cortex for further processing (Figure 1A).

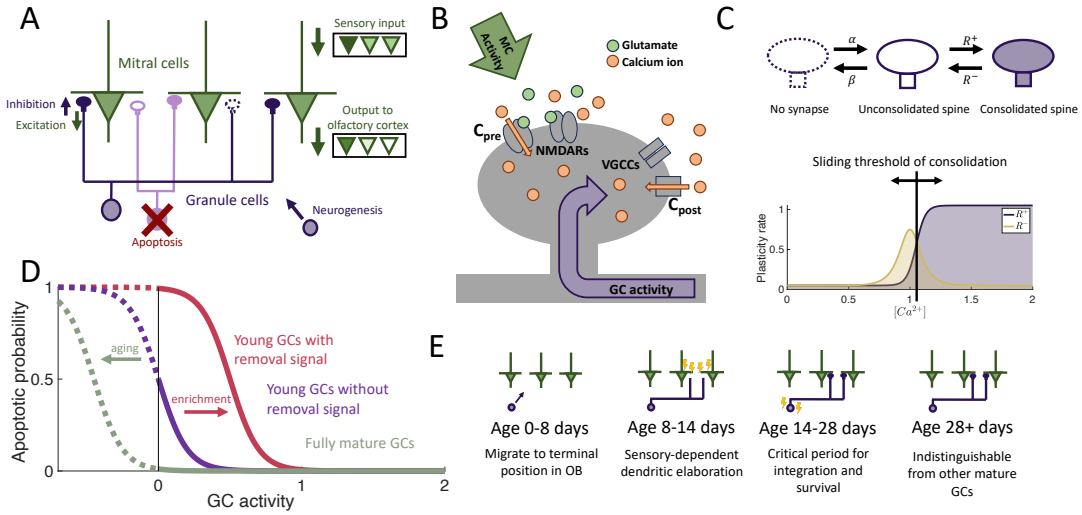

Figure 1. Computational model. (A) MCs relay stimuli to cortex. Reciprocal synapses with GCs can be functional or non-functional (cf. Fig.1C). Adult neurogenesis adds GCs and apoptosis removes GCs. (B) Calcium controls synaptic plasticity (cf. ***Graupner and Brunel*** (***2012***)). Influx into spine through MC-driven NMDARs and through voltage-gated calcium channels (VGCC) opened by global depolarization of GCs. (C) Unconsolidated spines are formed with rate α and removed with rate β. Spines become consolidated with a rate R^+ and deconsolidated with rate R^- (Top). $R^\pm$ depend on the local calcium concentration in the spine (Bottom). (D) GCs are removed with a rate that depends on activity and age of the cells, as well as environmental factors (see Methods). (E) Development of abGCs. At age 8-14 days they integrate silently into the OB. The formation and elaboration of their dendrites depends on sensory input. During their critical period (14-28 days) the abGCs are more excitable and plastic and have a higher rate of apoptosis. Beyond 28 days the abGCs are mature GCs.

The sparse structural characteristics of the dendritic networks were incorporated within both the MC and GC populations by allowing each GC to form synaptic connections with only a subset of MCs. The MC-GC synaptic network was persistently modified by activity-dependent structural synaptic plasticity in which synapses located on GC dendrites were formed and eliminated ***Livneh and Mizrahi*** (***2012***); ***Sailor et al.*** (***2016***). Because such structural plasticity is known to rely on the local calcium concentration at the spine ***Kasai et al.*** (***2021***), we adapted a previously published model that approximates the calcium concentration at each synapse as a function of pre- and post-synaptic activity ***Graupner and Brunel*** (***2012***) (Figure 1B and Synaptic Plasticity in Methods)

The synaptic dynamics were modeled with a Markov chain consisting of three states: non-existent, unconsolidated, and consolidated (Figure 1C). Non-existent synapses represent locations where a synapse between an MC and a GC is geometrically possible but not realized. Unconsolidated synapses represent filopodia, silent synapses, or unconsolidated spines that provide a foundation for a functional synapse but do not yet generate a postsynaptic response. Finally, consolidated synapses represent fully functional connections. We assumed that synapses transition between the unconsolidated and non-existent states at a constant rate, independent of activity. Conversely, transitions between unconsolidated and consolidated synapses occured with an activity-dependent rate so that sensory experience shapes the functional connectivity of the network. This assumption arises from experimental findings that GC spine dynamics depend on GC activity ***Breton-Provencher et al.*** (***2014***, 2016); ***Saha et al.*** (***2021***).

In the OB, apoptosis is activity-dependent ***Benson et al.*** (***1984***); ***Yamaguchi and Mori*** (***2005***); ***Lin et al.*** (***2010***); ***Yokoyama et al.*** (***2011***) with young abGCs more susceptible than mature GCs ***Yamaguchi and Mori*** (***2005***). Furthermore, the survival of abGCs has been shown to be modulated by behavioral state ***Yokoyama et al.*** (***2011***); ***Yamaguchi et al.*** (***2013***); ***Komano-Inoue et al.*** (***2014***) and impacted by enrichment with novel, but not with familiar odors ***Veyrac et al.*** (***2009***). Therefore as

a minimal model of apoptosis, we assumed that fully mature GCs had a low threshold of activity required for survival, while young abGCs had a higher threshold. In addition, the latter were susceptible to an apoptotic signal that was triggered by olfactory enrichment, which further raised the threshold, similar to the two-stage model for GC elimination proposed by ***Yokoyama et al.*** (***2011***); ***Yamaguchi et al.*** (***2013***); ***Komano-Inoue et al.*** (***2014***) (Figure 1D).

To investigate the role of the aforementioned transient properties of newly arrived abGCs (summarized in Figure 1E), we evaluated the network's performance in a perceptual learning task (Figure 2B). In this task, the network is repeatedly presented with alternating, similar artificial stimuli ("enrichment") and assessed in its ability to discriminate between these stimuli by comparing their MC-representations. We quantified this discriminability in terms of the Fisher discriminant (Discrimination in Supplementary Information). The enhancement in discriminability parallels the formation of an odor-specific network structure. We therefore quantified the memory in terms of the specificity of that connectivity (cf. Memory in Methods).

Age-dependent plasticity and excitability reconcile flexibility and stability of memory

In order to establish what can be gained from the addition of new neurons alone, we initially disregarded apoptosis and the transient properties of abGCs, resulting in a baseline model of adult neurogenesis where a homogeneous population of GCs grew over time. In Figure 2C we simulated the perceptual learning experiment using neurogenic (solid lines) or non-neurogenic (dashed lines) networks comprising either uniformly fast (green) or slow (blue) synapses. There was no significant difference between the results of the neurogenic and non-neurogenic models, so neurogenesis alone did not impact learning or memory.

Due to the pivotal roles of plasticity rates in memory encoding, we first explored the impact of the differing rates of synaptic plasticity in young and old GCs (Figure 2A). The rates of spine turnover were calibrated to align with empirical data ***Sailor et al.*** (***2016***) (Figure SI1A). This transiently enhanced plasticity partially resolved the flexibility-stability dilemma, as the age-dependent network encoded memories more swiftly than the network of slow synapses while maintaining greater stability than the network with fast synapses (Figure 2C, red curves). Thus, the heightened plasticity of young abGCs allowed them to rapidly encode new memories and retain them as the neurons matured and their plasticity rate decreased.

We repeated this simulation while incorporating the increased excitability of abGCs in their critical period (Figure 2D). The age-dependent excitability provided the benefit of increasing the initial memory of the model (Figure 2E, red curve) to the full strength of the fast network, while retaining the stability of the slow network. Importantly, this only occurred in conjunction with age-dependent plasticity and not in the networks with constant plasticity rates (Figure 2E, blue and green curves). Thus, the increased excitability in young abGCs cooperates with their increased plasticity to improve the initial memory of the OB.

Models of adult neurogenesis often have a common drawback: as the networks grow, their performance tends to decrease due to greater interference by the accumulating adult-born neurons ***Meltzer et al.*** (***2005***); ***Aimone et al.*** (***2011***); ***Kudithipudi et al.*** (***2022***). We hypothesized that the increased excitability of young abGCs may mitigate this effect by raising the activity of abGC synapses that would otherwise be quieted through lateral inhibition from the vast population of mature GCs. To test this, we conducted a simulation where the onset of enrichment was progressively delayed, allowing an increasing number of GCs to accumulate in the OB (Figure 2F). We carried this out in cases with and without enhanced excitability of young abGCs. The network featuring age-dependent excitability substantially outperformed the network without this feature (Figure 2G). Thus, the transiently enhanced excitability of abGCs contributed to maintaining the learning flexibility of the OB in the face of persistent neurogenesis.

To better understand how memories were encoded in the OB, we analyzed the MC-GC connectivity immediately following enrichment. We performed hierarchical clustering on the columns

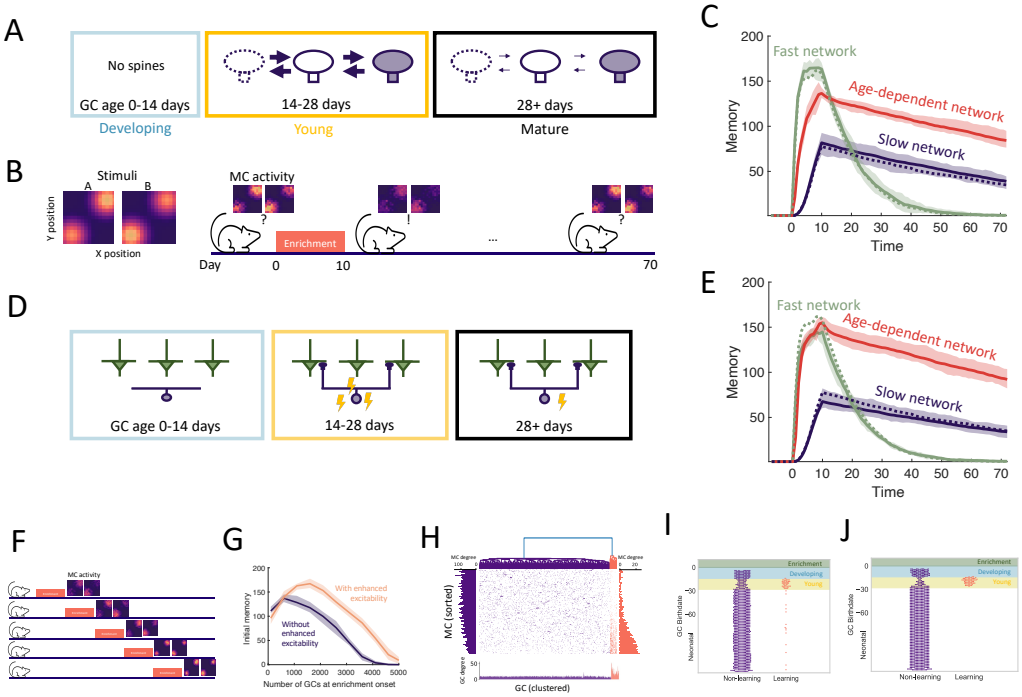

Figure 2. Age-dependent plasticity. (A) AbGCs in their critical period (14-28 days) exhibit greater spine turnover. (B) Left: Activity of MCs arranged on a two-dimensional grid and stimulated with stimulus A or B, respectively. Right: MCs initially respond similarly to both stimuli, but responses diverge after a 10 day enrichment. Over time, spontaneous synaptic changes lead to forgetting. (C) Memory is measured as a function of the network connectivity (see Methods) for three different models: neurons with fast plasticity (green), neurons with slow plasticity (blue), neurons with age-dependent plasticity (red). Dashed curves are networks without neurogenesis. Lines: mean memory across eight trials, shaded areas: full range. The memory evolution is similar to that of the odor discriminability as measured using the Fisher discriminant (Figure SI1B). (D) abGCs exhibit also increased excitability during their critical period. (E) The initial memory is enhanced by the increased excitability. (F) Delayed enrichment simulation in which the model was allowed to grow for longer and longer times preceding enrichment. MC responses to the test odors show diminished learning for delayed enrichment. (G) The memory immediately following enrichment as a function of the number of GCs at enrichment onset for the case with (orange) and without (purple) age-dependent excitability. (H) MC-GC connectivity at the end of the enrichment period of one simulation; orange: odor-specific connectivity ('learning' GCs), purple: unspecific connectivity ('non-learning'). Center: connectivity matrix. Top: dendrogram reflecting hierarchical clustering of GCs according to their connectivity. Bottom: number of connections of each GC. Sides: number of connections of each MC to learning and non-learning GCs, respectively. (I,J) Birthdates relative to enrichment onset of learning (orange) and non-learning (purple) GCs for models without and with increased excitability, respectively. At enrichment onset GCs in the blue and yellow regions were in the developing and young stages, respectively (Figure 2A). Green region shows enrichment period. Only GCs that were incorporated into the OB network (age > 14 days) at the end of enrichment are shown. $N_{conn} = 100$ and $R_0 = 0.005$ were used for all simulations in this figure.

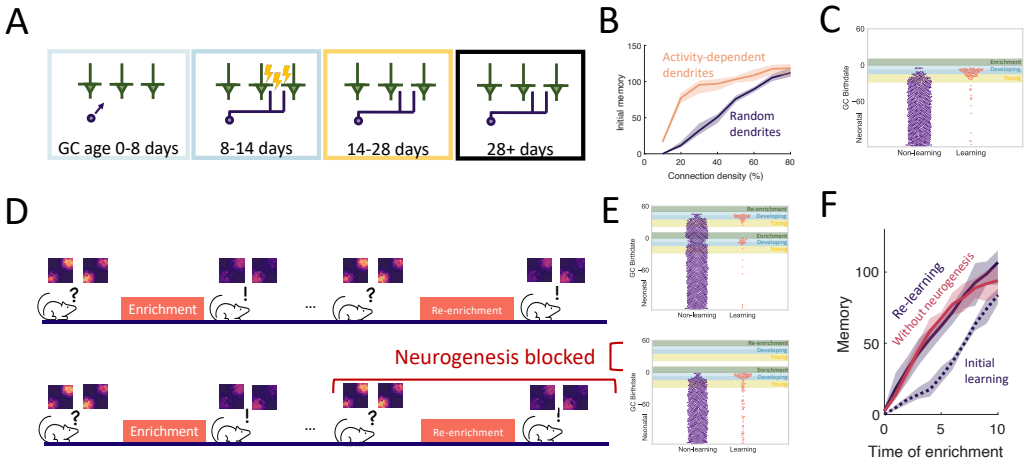

Figure 3. Dendritic structure. (A) Sensory-dependent silent integration of juvenile abGCs (cf. Fig.2A,D and Methods). (B) Memory following enrichment as a function of the number of potential synapses with random (purple) and activity-dependent (orange) dendritic elaboration. (C) Birthdate analysis as in Figure 2I. Learning mostly by abGCs that develop their dendrites during enrichment (blue region). (D) Enrichment was followed by a period of spontaneous activity until the memory cleared, then re-enrichment occurred with the same set of stimuli. (E) Birthdate analysis with a second set of colored regions corresponding to the re-enrichment (cf. Figure 3C). (F) Memory evolution during the initial enrichment (dotted line) and second enrichment both with (purple solid line) and without (orange solid line) neurogenesis. Lines: average across eight trials, shaded region: entire range of values.

of the connectivity matrix in order to cluster GCs into groups of similar connectivity. There were two distinct clusters: a large portion of GCs were non-specifically connected (purple in Figure 2H), while others exhibited an increased total number of synapses and were preferentially connected with MCs that responded strongly to the enrichment odors (orange in Figure 2H). Cluster membership was then sorted by GC birthdate relative to enrichment, which revealed that abGCs that were young at the beginning of the enrichment period (yellow shaded area) were preferentially recruited to the learning cluster (Figure 2I), This degree of preferential recruitment was increased through the transient hyperexcitability (Figure 2J). Thus, synapses of odor-responding MCs were redistributed from the non-learning cluster to the learning cluster (Figure 2H, vertical MC degree bar plots). This is similar to findings in the hippocampus that young adult-born neurons both add new synapses to the network and replace existing synapses formed by mature GCs ***Adlaf et al.*** (***2017***).

Notably, even with increased initial excitability abGCs that arrived in the OB during the enrichment phase (blue area) made only a minimal contribution to the memory (Figure 2I,J). This conflicted explicitly with the experimental finding that the silencing of these abGCs extinguishes this memory ***Forest et al.*** (***2019***, 2020). We therefore asked whether this discrepancy could be reconciled by considering additional known developmental properties of abGCs.

The dendritic structure of abGCs latently encodes memories

An important aspect of GC development is the period of dendritic development when newborn neurons are integrating silently into the OB. Because of experimental evidence that the elaboration of distal dendrites of abGCs depends on sensory input ***Saghatelyan et al.*** (***2005***); ***Yoshihara et al.*** (***2012***, 2016), we biased the dendritic field of abGCs such that abGCs were more likely to have potential synapses with MCs that were more active when the GC was 8-14 days old (Figure 3A). While this did not substantially affect flexibility or stability of the network (Figure S2A), it allowed the model to achieve strong memories even when the GCs could only connect to a small fraction of all MCs, consistent with the sparse connectivity of the bulb (Figure 3B). More importantly, it led

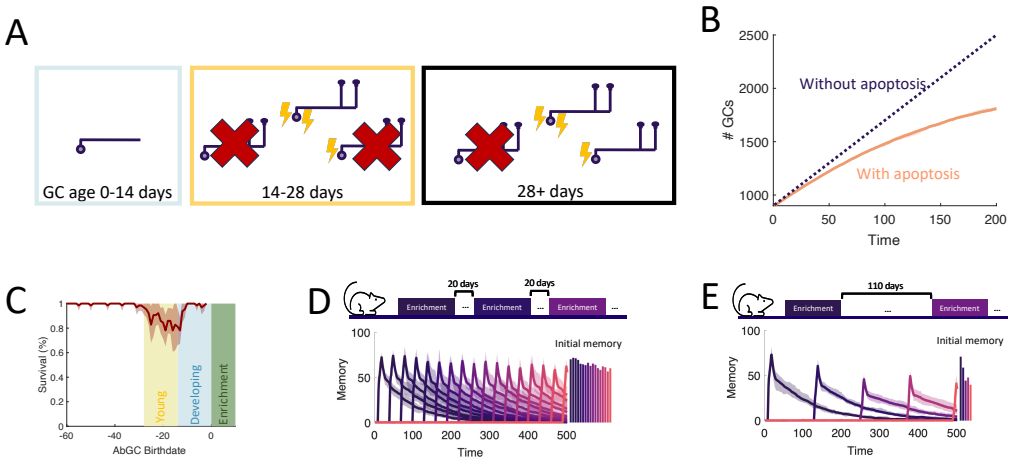

Figure 4. Apoptosis. (A) AbGCs in their critical period (14-28 days) require a higher level of activity to survive. (B) The growth of the GC layer over time. (C) The portion of surviving GCs as a function of birthdate. The shaded regions are as in Figure 2E. Line: average across eight trials, shaded area: mean ± standard deviation. (D, E) Sequential enrichment simulations differing in the inter-enrichment interval. Each curve corresponds to the mean memory of a stimulus over eight trials and the shaded areas show the range over all trials. The bar plots show the mean initial memory for each stimulus.

to the preferential recruitment of abGCs that arrived in the OB during enrichment (Figure 3C, blue areas) over those that arrived just before enrichment (Figure 3C, yellow area). This matches the experimental results, which show that these abGCs encode the memory ***Forest et al.*** (***2019***, 2020).

We also examined the savings effect ***Ebbinghaus*** (***1885***) in which the re-learning of forgotten information occurs more rapidly than the initial learning. This effect has been observed in an olfactory associative learning task, where abGCs seem to be playing a significant role ***Sultan et al.*** (***2010***). We examined this in our perceptual learning framework by simulating a similar relearning experiment and exploring what happens if neurogenesis is blocked during relearning (Fig. 3D). The model predicts that GCs that initially encoded the memory are re-recruited to the odors during re-enrichment (Figure 3E). While these GCs were no longer as highly excitable or plastic as young GCs, they had the advantage that their dendritic fields overlapped strongly with MCs that are excited during enrichment, allowing them to efficiently re-establish their synaptic connections. This led to savings where the memory increased more rapidly during the re-enrichment (Figure 3F).

Additionally, despite the fact that neurogenesis is typically required for learning, the model predicts that savings will be seen even if neurogenesis is blocked during the second enrichment (Figure 3E, F). Importantly, these observations did not occur without the activity-dependent dendritic elaboration of young abGCs (Figure SI2B), meaning the dendrites encoded "latent memories" that facilitated the rapid re-expression of a previously encoded memory upon re-exposure to the stimulus.

Targeted apoptosis maintains flexibility

The final property of GC development that we investigated is the death of GCs through apoptosis, which is heightened for abGCs in their critical period (Figure 4A). This critical period of survival led to two noteworthy phenomena. First, when tracking the growth of the OB, the number of GCs initially grew approximately linearly, while growth eventually started to slow down (Figure 4B), as observed experimentally ***Platel et al.*** (***2019***). Second, there was a high rate of apoptosis in older young abGCs (Figure 4C, yellow area) in response to olfactory enrichment but not in abGCs that arrived in the OB during enrichment (blue area) or mature GCs (unshaded area). This is similar to

experimental results that show enhanced death of 'middle-aged' abGCs, but not young or more mature abGCs ***Mouret et al.*** (***2008***).

What are the potential implications of apoptosis on memory encoding? One known outcome is that it subjects newly formed memories to retrograde interference ***Forest et al.*** (***2019***). In these experiments, there were two enrichment periods with odors that activated largely non-overlapping sets of GCs. If the second enrichment occurred while abGCs that encoded the memory of the first enrichment were still in their critical period, then these abGCs succumbed to apoptosis and the memory was extinguished. Our model captured this and identified that the dissimilarity of the odors is essential (Figure SI4): because the connectivity developed by the odor-encoding GCs during the first enrichment was odor-specific, these GCs were inactive during the second enrichment and therefore more susceptible to apoptosis. If, alternatively, there was a long enough gap between the enrichment periods, or if the odors from the first enrichment were present during the second enrichment, then the abGCs encoding the first memory survived and the memory was consolidated in both the model and experiments. This highlights how apoptosis can selectively remove abGCs, and how only naive, young abGCs are available to encode new odors.

Yet the question still remains if apoptosis can facilitate the formation of new memories rather than exclusively eliminate old ones. Based on the observation in Figure 2G that the ability to form new memories declined as the number of GCs grew, we hypothesized that apoptosis may help sustain the flexibility of memory formation as adult neurogenesis persists. To test how well the network learned under different levels of apoptosis, in Figure 4D,E the network was enriched with a variable number of equally-spaced enrichments consisting of sparse, random odors (Figure SI3A) over the same time interval. Because enrichment cleared a large portion of abGCs that were late in their critical period at enrichment onset (Figure 4C), we expected to see more apoptosis and thus improved learning in trials with a greater number of enrichments. Indeed, when there were many enrichments, the network flexibly learned all odors similarly well (Figure 4D), but when there were fewer enrichments, the initial memory strength of later odors decreased substantially as neurons accumulated in the OB (Figure 4E). As a result, the model predicts that long periods without olfactory enrichment or with apoptosis blocked negatively impact the ability to learn new odors.

Adult neurogenesis supports life-long learning

To study the capacity of the OB to continually encode new stimuli, we simulated an experiment where we sequentially enriched the OB network on twenty-five sparse, random odor pairs (Figure 5A) and measured how the properties of the memories change over time. Our full model of the OB supported the flexible encoding of stable memories (Figure 5B). Learning flexibility, measured as the initial memory of the enrichment odors, was strongest at the start of the simulation; but it declined only slightly in subsequent enrichments and approached a steady value when the growth of the network started to saturate. Additionally, memories remained stable: the decay of the individual memory traces was barely affected by subsequent, interfering enrichments. This resulted in multiple odors having substantial memories at the final time of measurement, and these memories were graded according to the time of acquisition.

To show what properties of the OB are required to produce these results, we repeated the simulations under several different model conditions. First, in Figure 5C, we blocked apoptosis. While memories still remained stable, flexibility suffered greatly as the network eventually failed to learn. Notably, the memories of early enrichments were not strongly impacted, indicating that short-term suppression of apoptosis should not affect learning, consistent with observations ***Mouret et al.*** (***2009***). Next, we additionally removed the enhanced excitability of young abGCs (Figure 5D). Not only did flexibility decline more substantially, but memory stability also suffered as larger drops (see arrows) were evident in the individual memory traces during later enrichments. Finally, we considered a non-neurogenic network featuring only synaptic plasticity and none of the transient properties of abGCs (Figure 5E). While this network could flexibly form new memories, they were not stable as each subsequent enrichment led to the overwriting of old memories, severely limiting

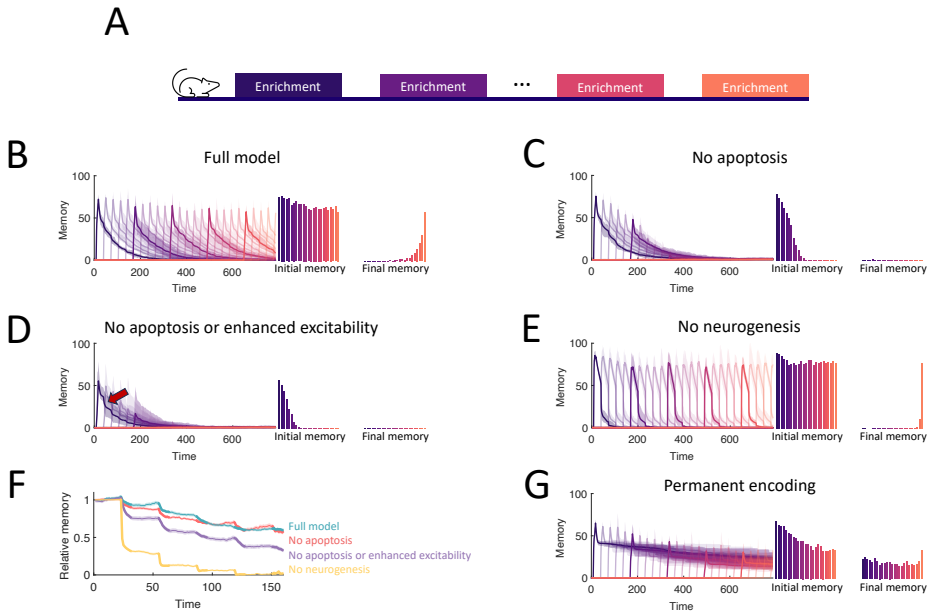

Figure 5. Neurogenesis for life-long learning. (A) Protocol for sequential enrichment simulations. (B-E) Memory evolution of full model, model without apoptosis, model without apoptosis or age-dependent excitability, and model without neurogenesis, respectively. Each curve corresponds to the memory of a different set of stimuli, with every fifth curve bolded for visualization. First bar plot plots show the mean initial memory, while the second bar plot shows the mean memory at the end of the simulation. Lines: average across eight trials, shaded areas: range over all trials. In (E), $p = 0.15$ and $R_0 = 0.003$ so that the model learns and forgets at a rate similar to that of the full model. (F) Memory of the first enrichment in (B)-(E) relative to the memory of that same enrichment without subsequent enrichments. Lines: average across trials, shaded area: standard error of the mean. Bolded segments correspond to times when the model is exposed to a new stimulus. (G) Memory for sequential enrichment if the connectivity of mature abGCs is frozen.

the memory capacity.

To evaluate quantitatively how the memory that was formed in the first enrichment deteriorated due to the ongoing encoding of new odors, we compared the memory traces of the first enrichment in Figure 5B-E to the memory trace of the same odor, but without any subsequent enrichments. Taking the ratio between these two traces shows the extent to which new stimuli overwrote old memories (Figure 5F, bolded segments correspond to enrichment periods). The non-neurogenic model displayed the most overwriting, with prominent overwriting events during the first few enrichments. Next, the network without the transiently enhanced excitability of young abGCs featured a moderate amount of overwriting, as young abGCs were no longer preferentially recruited to learn new odors. Finally, the full model and the model without apoptosis featured similarly low levels of overwriting, indicating that apoptosis is required for memory flexibility but not stability.

Because of the low degree of overwriting occurring in our full model of the OB, memory decay was primarily due to spontaneous synaptic changes. A large degree of spine turnover has been observed at MC-GC synapses in response to spontaneous activity alone, even on mature GCs ***Livneh and Mizrahi*** (***2012***); ***Sailor et al.*** (***2016***). We investigated the implications of this by comparing the results of the full model (Figure 5B) to those of a model of the OB in which plasticity was instead completely prevented in older GCs (Figure 5G). In this model, new memories briefly decayed due to spontaneous plasticity in young abGCs, but then were maintained for the duration of the simulation. Although there was explicitly no synaptic overwriting, the memories still featured a slow decay due to the apoptosis of odor-encoding GCs. Apoptosis was more prominent in this network because the odor-encoding neurons featured a larger number of synapses (Figure 2H) that would otherwise be reduced through spontaneous plasticity. Thus, there was a greater degree of inhibition in the network, reducing GC survival. Importantly, these excess synapses lead to more interference, which degraded the flexibility in this network (cf. initial memories in Figure 5B, G). This suggested that the strong synaptic fluctuations among mature GCs served to increase flexibility by removing potentially interfering, un-maintained memories of odors. Of course, this strategy has the drawback that memories are less stable, but this drawback is mitigated by the latent memories of the odors being stored in the dendrites of abGCs, which allow for their rapid re-acquisition if the odors are once again present in the environment (Figure 3).

Discussion

Here, we showed a clear computational advantage of adult-neurogenesis in ongoing memory encoding. In a computational model of the OB, the increased plasticity exhibited by abGCs in their critical period allowed them to rapidly encode new information, while their subsequent development and the resulting decrease in plasticity rate ensured that the memories they encode remain stable. Meanwhile, the increased excitability of young abGCs enhanced their preferential recruitment in learning new information, while also helping maintain the flexibility of the system as new neurons accumulate in the OB. Apoptosis similarly helped maintain learning flexibility through the targeted removal of abGCs that fail to learn the odors presented during their critical period. Furthermore, the activity-dependent dendritic elaboration of juvenile abGCs led to pre-configured sub-networks of similarly aged abGCs that enabled the rapid re-acquisition of memory. All of these elements were required to reproduce the relevant experimental results.

Other models addressing the flexibility-stability problem

From a signal-theoretic perspective, both initial strength and duration of a new memory should improve as synapses are added to the network. Due to the metabolic cost of forming and removing synapses it is important to use them efficiently. This is especially true for neurogenic systems in which the increase in the number of synapses is associated with the addition of new neurons. The efficiency of the system can be characterized by how strongly its memory performance increases when the number N of synapses is increased.

To assess this efficiency, we adapted a framework proposed by ***Fusi et al.*** (***2005***); ***Roxin and Fusi*** (***2013***) to analyze how memories degrade in response to ongoing plasticity (Supplementary Information SI2). In systems where both learning and forgetting occur on the same, fast time scale the overall memory capacity grows only logarithmically with N ***Amit and Fusi*** (***1994***); ***Fusi and Abbott*** (***2007***). However, our computational model predicted that a network with age-dependent plasticity rates can have a vastly larger memory capacity on the order of $\sqrt{N}$ (cf. Supplementary Information SI2). This emphasizes not only that the augmented capacity of the model predominantly arises from the transiently increased plasticity rather than the mere addition of synapses, but also that this model efficiently uses the new synapses provided by adult neurogenesis.

These results are commensurate with earlier models specifically designed to address the flexibility-stability dilemma, particularly the classical cascade model ***Fusi et al.*** (***2005***) and the partitioned-memory model of systems consolidation ***Roxin and Fusi*** (***2013***) (Figure SI6). However, our model does not yield an increase in memory duration that is linear in N as demonstrated by the more complex bidirectional cascade model ***Benna and Fusi*** (***2016***). This difference underscores the intricate interplay of synaptic plasticity mechanisms and their impact on memory consolidation.

Why neurogenesis?

If there exist alternative methods that are theoretically demonstrated to consolidate memory with comparable effectiveness ***Fusi et al.*** (***2005***); ***Roxin and Fusi*** (***2013***); ***Benna and Fusi*** (***2016***), why does the OB opt for adult neurogenesis? Adult neurogenesis is a rare phenomenon in mammals, but more common in organisms with less complex nervous systems, such as reptiles, birds, and fish. This contrast suggests an evolutionary pressure to reduce neurogenesis that is resisted by the OB ***Aimone*** (***2016***). To understand why neurogenesis is nevertheless favored in the OB, it is crucial to examine the specific function of the OB and its constituent GCs.

One of the observed functions of the OB is the enhancement of small differences between similar stimuli ***Gschwend et al.*** (***2015***). The lateral inhibition between MCs that is mediated by GCs plays a key role in this function ***Wick et al.*** (***2010***); ***Wiechert et al.*** (***2010***); ***Koulakov et al.*** (***2011***). This processing is similar to contrast enhancement and edge enhancement performed in visual processing by the retina ***Hartline and Ratliff*** (***1957***). Since natural visual objects are always contiguous, the input that neighboring 'pixels' in the retina receive are quite strongly correlated, regardless of the specific visual scene. For such statistics, low-level processing of the stimuli is possible with a pre-wired, spatially-dependent connectivity that provides interactions between *spatially* neighboring 'pixels'.

Olfactory stimuli, however, are extremely high-dimensional and do not have this topographic correlation structure. Even if the activation patterns of similar olfactory stimuli differ only in neighboring 'olfactory pixels' in this high-dimensional space, their projection onto the two-dimensional arrangement of glomeruli results in 'fragmented' activation patterns, wherein the relevant 'olfactory pixels' are widely distributed across large portions of the bulbar surface ***Cleland and Sethupathy*** (***2006***); indeed, experiments have shown that the receptive fields of glomeruli provide only little information about those of nearby glomeruli ***Soucy et al.*** (***2009***). Therefore, seemingly random, spatially widespread 'olfactory pixels' exhibit correlations, and the specific set of correlated pixels depends sensitively on the specific stimuli the animal experiences. Local processing that does not take these correlations into account can provide initial contrast enhancement ***Cleland and Sethupathy*** (***2006***). It is, however, limited in its scope and computations that aim to incorporate the correlation structure require lateral connectivity as it is provided by GCs.

Only a subset of odors is innately relevant and has the same meaning for all animals of a given species and can likely be processed with a fixed, pre-wired connectivity. However, odors that provide, e.g., kinship or pup recognition differ from individuum to individuum. Each animal must accordingly learn how to process these odors on-demand when they become relevant, which is often not until the animal is mature. The OB must therefore allow for life-long learning.

For life-long learning, the flexible learning of new stimuli while maintaining the stability of

old memories is crucial. Our modeling demonstrates that neurogenesis and the development of abGCs provide exactly this. However, we also showed that both the survival of too many memories and of too many GCs can harm the flexibility of the network. This raises the question of which memories and GCs should endure and for how long. Previous experiments and our modeling show that after an odor is learned, the abGCs recruited to that odor are subject to retrograde interference during their critical period: unless the initial odor is maintained in the environment the learning of a new memory decreases the survival of the abGCs associated with the earlier odor ***Forest et al.*** (***2019***).

Past their critical period, the abGCs are much more stable. Nevertheless, the animals lose the memory of the learned odor over the course of 30-40 days ***Forest et al.*** (***2019***). However, at that point they can re-acquire that memory faster than they had learned it initially ***Sultan et al.*** (***2010***). This is consistent with the relevant synaptic connections being lost, reflecting the strong spontaneous formation and removal of GC spines ***Sailor et al.*** (***2016***); ***Meng and Riecke*** (***2022***), while the relevant GCs are still present and provide through their stable dendrites ***Mizrahi*** (***2007***); ***Sailor et al.*** (***2016***) a latent memory that can quickly be reactivated by reforming the relevant synapses.

What controls the survival of GCs over yet longer times is not quite clear. In ***Sultan et al.*** (***2010***) the GCs die over the course of 90 days in the absence of the odor they memorized. In the experiments of ***Platel et al.*** (***2019***), however, animals were not exposed to any tasks and little if any cell death is reported. From a functional point of view, the long-term survival of odor-encoding abGCs in the absence of further exposure to the memorized odor is expected to be controlled by the need to avoid interference with new odors while accommodating the possibility that the same odor will reappear at some later point in time. In principle, a sufficiently similar odor could become relevant, which would favor the persistence of these GCs. However, the vast dimension of odor space makes the latter unlikely and suggests that on a longer time scale GCs should be removed by apoptosis. Thus, our modeling suggests that the high dimension of odor space together with the need for animals to learn specific odors quickly but stably strongly favors structural plasticity through adult neurogenesis and apoptosis.

Relation to adult neurogenesis in the hippocampus

Adult neurogenesis also occurs in granule cells in the hippocampus ***Christian et al.*** (***2014***); ***Kempermann et al.*** (***2015***). Like olfactory abGCs, hippocampal abGCs exhibit transiently increased plasticity and excitability ***Lledo et al.*** (***2006***); however, they are excitatory and constitute the principal neurons of their network. Hippocampal GCs contribute to pattern separation and memory acquisition much like olfactory GCs, but also play an important role in other aspects of spatial and contextual memory ***Aimone et al.*** (***2009***); ***Christian et al.*** (***2014***).

On the topic of memory stability, recent experiments have shown that up-regulating hippocampal neurogenesis can enhance the forgetting of previously learned information over the course of a month, while down-regulating it can diminish the forgetting ***Akers et al.*** (***2014***). This suggests that interference from new cells makes old memories unstable and aids in memory clearance ***Akers et al.*** (***2014***); ***Epp et al.*** (***2016***); ***Gao et al.*** (***2018***); ***Guskjolen and Cembrowski*** (***2023***). Computational modeling and experiments have suggested that this forgetting may specifically be happening at the mossy fiber-CA3 synapse ***Tran et al.*** (***2019***); ***Guskjolen et al.*** (***2023***).

In our model, while abGCs born after learning cause interference in the network and perturb MC responses, only a vast increase of the post-learning neurogenesis rate would significantly alter the memory duration (Figure SI5). Our research suggests a different role for adult neurogenesis: the age-dependent properties of the abGCs can stabilize memories for more than a month that would otherwise decay over the course of a week (Fig.2B). In view of the metabolic costs of neurogenesis, this would seem to be a better investment than memory clearance.

The development of birthdate-dependent subnetworks

A key outcome of our model is the development of birthdate-dependent odor-specific subnetworks. This applies not only to the synaptic networks, but also to the underlying dendritic networks. In the model, this is because abGCs born in a similar time window begin development in a similar environment. We therefore predict that the rapid re-learning observed in an olfactory associative learning task ***Sultan et al.*** (***2011***) would also occur in a perceptual learning experiment and would still be present even if neurogenesis was blocked after the initial enrichment.

This would be notable for two reasons. First, it has been shown that neurogenesis is required for perceptual learning of fine odor discrimination ***Moreno et al.*** (***2009***). Therefore, if re-learning were to occur without neurogenesis, then it would indicate that there is some structure storing a latent memory that is not expressed behaviorally. Second, the fast re-learning was not seen in the model without activity-dependent dendritic elaboration, so it would suggest that the dendritic tree may be a substrate of this latent memory. Importantly, these latent memories only persist as long as the neurons encoding them survive. It remains to be seen if periodic re-exposure to stimuli after learning can extend the lifetime of odor-encoding abGCs, as would be expected in a model where the OB predominantly eliminates GCs that encode extraneous information.

Similar results of birthdate-dependent subnetworks have been observed experimentally as a result of embryonic neurogenesis in the hippocampus ***Huszár et al.*** (***2022***). In this study, place cells in CA1 were observed to form assemblies where neurons were more likely to be in the same assembly with other neurons born on the same day compared to those born on different days. Importantly, in a place alternation task, these cells have also been observed to remap together, maintaining sub-assemblies across environments. In this sense, the hippocampal neurons exhibited a set of pre-configured activity patterns dependent on their birth-date, reminiscent of the latent memories we describe in our model.

The role of apoptosis in learning

In addition to predictions about relearning, the model predicts that apoptosis helps maintain the flexibility of the OB and that reduced apoptosis would lead to memory deficits (Figure 4, Figure 5C). In standard, non-enriched laboratory conditions, the observed rate of apoptosis of abGCs after they have established themselves in the OB network is low ***Platel et al.*** (***2019***). In such conditions, the model predicts that abGCs that fail to encode any relevant information accumulate in the OB and add non-specific inhibition to the OB, making it more difficult for new abGCs to integrate into the OB when new odors are presented.

Olfactory enrichment eliminates many abGCs that are late in their critical period that may otherwise survive ***Forest et al.*** (***2019***); ***Mouret et al.*** (***2008***). At the same time, it also enhances the number of abGCs that survive until they start integrating into the network, despite the unchanged proliferation rate ***Rochefort et al.*** (***2002***). The latter mechanism has not been built into the model, making it natural to wonder if this would impact the results in Figure 4. To address this, we doubled the number of new neurons available to integrate into the network during enrichment (Figure SI3) and found this did not qualitatively change the results.

We expect that the enhanced flexibility due to apoptosis would likely be most pronounced in mice between six and twelve months, when olfactory perceptual memory deficits start to appear ***Greco-Vuilloud et al.*** (***2022***) and the growth of the granule cell layer starts to slow down ***Platel et al.*** (***2019***). Indeed, very recently it has been observed that long-term olfactory enrichment improves memory in this cohort of mice ***Terrier et al.*** (***2024***).

Importantly, there are many other modulators of abGC survival beyond olfactory enrichment. For example, apoptosis can be induced by a variety of behavioral states ***Yokoyama et al.*** (***2011***); ***Yamaguchi et al.*** (***2013***); ***Komano-Inoue et al.*** (***2014***). In the natural world we would therefore expect to see a more substantial degree of apoptosis, which the model predicts to preserve the flexibility of the OB.

Model assumptions and outlook

In developing the computational model we have made a number of assumptions that are consistent with current experimental observations, but for which the underlying biophysical mechanisms are still poorly understood. The model therefore points to aspects of neurogenesis the experimental exploration of which would be particularly important in order to understand the functional relevance of adult neurogenesis.

We assumed that there exists an explicit removal signal that enhances apoptosis under certain experimental conditions such as olfactory enrichment. While experiments have shown that top-down inputs in response to different environmental or behavioral states may provide such an apoptotic signal ***Yokoyama et al.*** (***2011***); ***Komano-Inoue et al.*** (***2014***), how it precisely influences survival is not known. As a minimal model, we assumed that this signal shifts the survival curves (Figure 1D), but it is likely that apoptosis is a more complex process controlled by additional variables that are not yet well understood. Further investigation into the precise biological mechanisms that regulate apoptosis in the OB would be needed to inform more detailed models.

The precise details of the maturation of adult-born neurons are also not yet quite clear. We have assumed that the age-dependent parameters follow a simple step function with the step occurring on day 28 for each parameter. While this assumption simplifies the model, the age-dependent properties of abGCs may change continuously over the course of development. Furthermore, it is not clear if experience alters the timeline of development by altering the critical periods of integration and survival. It is possible that a lack of activity may slow down maturation, giving abGCs more time to integrate into the network or making them more vulnerable to apoptosis in order to avoid wasting resources.

An important part of the processing of olfactory stimuli is the spike timing information ***Wilson et al.*** (***2017***); ***Bolding and Franks*** (***2017***). Likewise, an important part of neural computation in general is the compartmentalization of the dendrites and soma. By modeling the neural activity with a single-compartment firing-rate model rather than a more complex spiking model, we neglect these important mechanisms and the information they convey. Our ideal observer approach of focusing on the network connectivity rather than the activity of the neurons circumvents this issue by providing an upper bound on the properties of memories in a more biologically plausible spiking model. Once sufficient information is available about the extent to which apoptosis depends on spiking dynamics and its compartmentalization a more refined model can be developed.

A prominent feature of olfaction is the extensive glutamatergic centrifugal input via top-down projections targeting GCs. We assumed that such input from higher brain areas could be ignored for our perceptual learning tasks; however, it may play a larger role in other tasks such as those involving associated context ***Mandairon et al.*** (***2014***). Computational modeling ***Adams et al.*** (***2019***) suggests that in such tasks, the bulbar component of the resulting learned connectivity features GCs developing odor-specific receptive fields with respect to their sensory and their top-down inputs. In this case, the top-down inputs selectively activate GCs that - through their reciprocal connections - inhibit specific MCs. This gives the top-down inputs, which can reflect non-olfactory contextual information, very specific control of the bulbar response to the associated odor. The plasticity investigated here leads to a network with a similar connectivity structure in the bulb. This would straightforwardly provide the substrate for such specific cortical control of odor processing.

Methods and Materials

Neuron model

We model the activity of MCs and GCs within a firing-rate framework,

$$\tau_M \frac{dM_i}{dt} = -M_i + [S_i - \gamma \sum_j w_{ij} G_j]_+, \tag{1}$$

$$\tau_G \frac{dG_i}{dt} = -G_i + r \sum_j w_{ji} M_j. \tag{2}$$

Here, M_i and G_i represent the firing rates of individual mitral cells and granule cells, respectively, and $[x]_+$ denotes a threshold-linear rectifier: $[x]_+ = x$ for $x > 0$ and $[x]_+ = 0$ for $x \leq 0$. The input to MC i consists of the sensory input S_i^{odor} and a term $S^{spontaneous}$, through which the MCs have spontaneous activity even without sensory input,

$$S_i = S^{spontaneous} + S_i^{odor} . \tag{3}$$

The synaptic weights w_{ij} are 1 if the synapse between MC i and GC j is fully functional and 0 otherwise. Note, that each synapse is reciprocal, with the strength of the inhibition by granule cells given by γ. The parameter r captures the excitability of granule cells. Throughout this study we set the number of MCs N_{MC} as 225, and the initial number of GCs N_{GC} as 900.

To simulate neurogenesis, at each time step N_{add} GCs were added to the synaptic network. We chose N_{add} to be 8 so that the ratio of new cells to existing cells would be consistent with experimental estimates ***Kaplan et al.*** (***1985***). These new neurons had dendritic spines and were immediately capable of providing inhibition, corresponding in mice to abGCs that are about 14 days old ***Carleton et al.*** (***2003***); ***Kelsch et al.*** (***2008***). To reflect the observation that young abGCs, aged 14 to 28 days, are more excitable than mature GCs, we made the parameter r age-dependent. For simplicity, we assumed this age dependence followed a step function, such that young cells had a high level of excitability and mature cells had lower one (Table 1).

Network structure

Because a GC can only form synapses with MCs whose dendrites come physically close to its own dendrites, we impose the restriction that GCs can only make synapses with a predetermined set of N_{conn} MCs. Since the MC dendrites extend across large portions of the olfactory bulb, we allowed connections between cells independent of the physical distance between somata. For neonatal GCs, this subset was randomly chosen. For abGCs, however, starting in Section “The dendritic structure of abGCs latently encodes memories", this subset was chosen in a semi activity-dependent manner to reflect the activity-dependent and -independent mechanisms which guide dendritic growth in developing cells ***Wong and Ghosh*** (***2002***); ***Saghatelyan et al.*** (***2005***); ***Dahlen et al.*** (***2011***); ***Yoshihara et al.*** (***2012***). To this end, we calculate a variable, $\tilde{M}_{i,j}$ that is used to determine which MCs i a given abGC j can connect to:

$$\tilde{M}_{i,j} = [\bar{M}_i - \theta_M]_+ + \varepsilon_{i,j}. \tag{4}$$

Here, $\bar{M}_i$ is the average activity of MC i over the 6 days preceding the addition of GC j to the network (corresponding to the amount of time between when an abGC arrives in the OB and when its starts spiking ***Carleton et al.*** (***2003***)), θ_M is the threshold of activity required to induce dendritic growth, and $\varepsilon_{i,j}$ is a random variable that mimics the complex structure of the MC dendrites and a random position of the GC soma relative to the set of MCs when it starts developing its dendritc arbor.

Whenever a GC j is added to the network, the set $\{MC\}_j^{(pot)}$ of MCs to which it can connect is given by the N_{conn} MCs that have the highest $\tilde{M}_{i,j}$ values at that time. Once a GC is added to the model, its set $\{MC\}_j^{(pot)}$ does not change; this is to reflect that dendrites of abGCs are relatively stable once the abGCs start spiking ***Mizrahi*** (***2007***); ***Sailor et al.*** (***2016***). Lastly, when GC j is added to the network it makes functional synapses with N_{init} MCs, randomly chosen from $\{MC\}_j^{(pot)}$. This applies to both neonatal and adult-born GCs.

Synaptic plasticity

We model synaptic dynamics as a Markov chain with three states: non-existent, unconsolidated, and consolidated. We include the unconsolidated state, since experimentally it is found that a substantial fraction of spines that are identified optically is lacking PSD-95 ***Saha et al.*** (***2021***). We assume state transitions from non-existent to unconsolidated occur randomly with a constant rate α and state transitions from unconsolidated to non-existent with constant rate β. Meanwhile, state

transitions to and from the consolidated state rely on pre- and post-synaptic activity. This assumption is supported by experiments as it has been shown that GC spine dynamics depend on GC activity **Breton-Provencher et al.** (**2014**, 2016); **Saha et al.** (**2021**). Moreover, the formation and removal of consolidated synapses appear to be separate processes that depend on the calcium concentration at the synapse **Kasai et al.** (**2021**); **Stein et al.** (**2021**); **Park et al.** (**2022**). Therefore we express the rate $R^+_{i,j}$ for the consolidation of an unconsolidated synapse between MC i and GC j and the corresponding deconsolidation rate $R^-_{i,j}$ as functions of a variable $[Ca]_{i,j}$ that mimics the calcium concentration at the synapse,

$$R^+_{i,j} = R_0 + \frac{1}{2}(\tanh(g([Ca]_{i,j} - \theta^+_j)) + 1) \tag{5}$$

$$R^-_{i,j} = R_0 + \frac{d}{\cosh(g([Ca]_{i,j} - \theta^-_j))}. \tag{6}$$

R_0 is the rate of spontaneous spine changes, g is a constant, and θ^+_j and θ^-_j are parameters related to the thresholds of spine formation and removal specific to GC j. Additionally, d is the relative rate of deconsolidation to consolidation, which we set to be less than one to reflect that consolidation is faster than deconsolidation **Kasai et al.** (**2021**).

The functional forms of these equations were chosen to qualitatively resemble those of the Artola-Bröcher-Singer (ABS) rule of synaptic plasticity **Artola et al.** (**1990**); **Artola and Singer** (**1993**) where highly active unconsolidated synapses are more likely to undergo consolidation **Vardalaki et al.** (**2022**) and less active consolidated synapses more likely to undergo deconsolidation **Kasai et al.** (**2021**). We further assume that each synaptic state is associated with a fixed weight value. Specifically, non-existent and unconsolidated synapses have synaptic weight zero, while consolidated synapses have weight one. We recognize that this approach ignores synaptic weight plasticity, but note that these binary synapses are representative of a class of realistic synaptic models **Fusi** (**2021**). Moreover, only limited information is available for the weight plasticity of MC-GC synapses **Gao and Strowbridge** (**2009**).

To model the local calcium concentration $[Ca]_{ij}$ at the synapse between MC i and GC j, we adapt the model presented by **Graupner and Brunel** (**2012**) to our firing rate framework:

$$\tau \frac{d[Ca]_{ij}}{dt} = -[Ca]_{ij} + C_{pre} r M_i + C_{post} G_j. \tag{7}$$

Here C_{pre} captures calcium influx driven by pre-synaptic activity: glutamatergic input from MC i and the resulting depolarization within the spine of GC j allow calcium influx through NMDARs and voltage-gated calcium channels. C_{post} captures calcium influx driven by post-synaptic activity that is independent of glutamate release from MC i: depolarization in the spine that is driven by (global) spikes in the GC dendrite allows calcium influx through voltage-gated calcium channels. The global spikes are reflected in the activity of GC j.

Next, we transform the rates $R^+_{i,j}$ and $R^-_{i,j}$ into state-transition probabilities through the functions

$$P^+_{ij} = 1 - \exp(-R^+_{i,j}), \tag{8}$$

$$P^-_{ij} = 1 - \exp(-R^-_{i,j}), \tag{9}$$

and stochastically consolidate synapses with probability P^+_{ij} and deconsolidate synapses with probability P^-_{ij}.

In order to maintain stability of the network, we impose a sliding threshold rule on the local consolidation parameters $\theta^\pm_j$,

$$\theta^+_j = \max(\theta^+, k[\bar{Ca}]_j), \tag{10}$$

$$\theta^-_j = \max(\theta^-, k[\bar{Ca}]_j), \tag{11}$$

where θ^+ and θ^- are the minimal thresholds for consolidation and deconsolidation respectively, k is a parameter, and $[\bar{Ca}]_j$ is the calcium concentration averaged across GC j. The sliding threshold represents intracellular competition between synapses.

Lastly, we scale all synaptic transition rates α, β, R^+ and R^- by a common plasticity rate p of the GC. To reflect the age-dependence of the plasticity rate, we make this parameter dependent on the age of each individual GC (see Table 1). The values of this parameter were chosen to match experimental data in ***Sailor et al.*** (***2016***) that measure spine turnover in GCs of different ages.

Apoptosis

We model apoptosis as an activity-dependent process where neurons are removed stochastically with probability given by the sigmoid

$$\mathcal{P}_i = \frac{1}{2}(1 - \tanh(5(G_i - G_0))). \tag{12}$$

Here $\mathcal{P}_i$ is the apoptotic probability of granule cell i and G_0 is an age-dependent survival threshold (Table 1). It reflects the fact that GCs are more susceptible to apoptosis in their critical period of survival ***Yamaguchi and Mori*** (***2005***), but still allows a small chance of apoptosis in mature GCs as observed experimentally ***Yokoyama et al.*** (***2011***). We model this by choosing the survival threshold G_0 to be higher for the immature abGCs than for the mature abGCs.

Recently, however, the degree of apoptosis has become controversial as it has been revealed that in standard conditions without any olfactory stimuli or behavioral task, there is in fact very little observed apoptosis (even for abGCs during their critical period) ***Platel et al.*** (***2019***). One potential explanation is that apoptosis is modulated by environmental and behavioral factors. Keeping with this, experiments have shown for example that survival of abGCs can be regulated by noradrenergic mechanisms in response to novel stimuli ***Veyrac et al.*** (***2009***). It has also been shown that apoptosis is more commonly observed during certain behavioral states ***Yokoyama et al.*** (***2011***); ***Yamaguchi et al.*** (***2013***); ***Komano-Inoue et al.*** (***2014***), and, when triggered, is enhanced in GCs receiving fewer sensory inputs ***Yokoyama et al.*** (***2011***). Moreover, GC survival can be increased by increasing the intrinsic excitability of the cells and relies on NMDARs ***Lin et al.*** (***2010***). Together, these results indicate that apoptosis depends on activity and age of GCs, as well as the environment and internal state of the animal. Therefore, to parsimoniously capture these results, we assume a "removal signal" occurs during enrichment that can cause young abGCs to be even more susceptible to apoptosis, raising the G_0 value for young cells further (Figure 1D). This mechanism is similar to the two-stage model for GC elimination proposed by ***Yokoyama et al.*** (***2011***); ***Yamaguchi et al.*** (***2013***); ***Komano-Inoue et al.*** (***2014***).

Memory

To assess the ability of the model to learn, we introduce an anatomic memory measure that is based on the network connectivity. Using an ideal observer approach, we assume that we have access to all synaptic strengths in the network. While the brain is unlikely to use such specific information to express memories, this gives us a limit on memory strength and duration and allows us to analyze how the OB network changes in response to olfactory enrichment.

We characterize the memory strength μ_i^s with which odor pair s is 'memorized' by GC i by the similarity (scalar product) between the average activity of MCs in response to that odor pair and the inhibition levied on those MCs by a unit activation of the GC i,

$$\mu_i^s = \sum_{j=1}^{N_{MC}} w_{ji} \bar{M}_j. \tag{13}$$

Here $\bar{M}_j$ is the mean activity of MC j in response to both odors in the pair s. This reflects the fact that the plasticity processes of the model lead to a network connectivity that provides mutual inhibition between MCs reflecting their co-activity in response to the training stimuli. We use both

odors in the pair s to characterize the memory, since, throughout this study, we examine how the network is able to learn to discriminate between two similar odors, which are both presented to the network in an alternating fashion.

We then define the total memory μ^s of odor pair s in the network as

$$\mu^s = \sum_{i=1}^{N_{GC}} [\mu_i^s - \theta_\mu(i)]_+. \tag{14}$$

Here, $\theta_\mu(i)$ is a threshold describing the "maximal null memory" of GC i. To obtain $\theta_\mu(i)$, we first determine the distribution of μ_i^s values for granule cell i across a set of 10,000 reshuffled connectivities. Then we take $\theta_\mu(i)$ to be 3 standard deviations above the mean of this distribution. This provides us with a measure how well the odor pair is encoded in the network above what would be expected from a random connectivity.

Clustering analysis

To characterize learning-induced subnetworks within the OB, we performed hierarchical clustering using an agglomerative approach with Ward linkage on the columns of the connectivity matrix between MCs and GCs ***Pedregosa et al.*** (***2011***). We then sought to identify the number of clusters present in the data using the resulting distances between groups of points returned by the algorithm. Due to the dependence of the clustering on the degree of the GCs, we did this using null distributions of the distances between groups found performing clustering on 10,000 shuffled networks, in the spirit of ***Johnson et al.*** (***2022***). This was done recursively. First we compared the distance between the two largest clusters in the data with the null distribution of distances between the largest clusters of shuffled data. If the true distance was outside of the distribution of shuffled distances then we deemed the cluster as significant and repeated the process on the two resulting subgroups. This continued until there were no new significant clusters.

Robustness and parameters

The full list of parameters of the model and their default values is found in Tables 1 and 2. The parameters C_{pre} and C_{post} were fit using the genetic algorithm `ga` ***The MathWorks Inc.*** (***2022***) to optimize memory following enrichment (Figure SI7A). The parameters α, β, and p were fit to match the rates of spine turnover in young and mature abGCs found by ***Sailor et al.*** (***2016***). Meanwhile, other parameters were tuned by hand to be consistent with more coarse experimental evidence. For example, R_0 controls memory decay due to spontaneous synaptic changes and was chosen such that memories endure for up to 30 days ***Forest et al.*** (***2019***). Since the forgetting may in part also be due to overwriting by other odors present, this value of R_0 may be somewhat too large. Additionally, the number of abGCs added each day, N_{add} was chosen so that the ratio $\frac{N_{add}}{N_{CG}}$ matched experimental estimates ***Kaplan et al.*** (***1985***). Still, several parameters had to be chosen without any available experimental support. Below is a discussion of a few selected parameters and their impact on the simulations.

The first parameters that we assessed were those associated with the abGC critical period (Table 1). The initial memory was robust to changes in the enhanced level of excitability of young abGCs, r, although learning declined slightly for the largest values we tested (Figure SI7B). We next examined the model's dependence on the survival threshold of young abGCs, G_0 (Figure SI7G). Increasing this parameter led to larger drops in the survival of abGCs that were already in their critical period at enrichment onset (yellow shaded area) without affecting the survival of most younger abGCs (blue shaded area), or the initial memory formed during enrichment.

We next explored the ramifications of other parameters associated with adult neurogenesis, starting with the neurogenesis rate, N_{add}. Unsurprisingly, reducing the neurogenesis rate leads to weaker memories, but as N_{add} is increased, the memory saturates (Figure SI7C). Our choice of N_{add} is in the saturated regime. We then looked at the noise parameter ϵ that represents the activity-independent component of dendritic elaboration (Figure SI7D). As would be expected, the amount

	Critical period	Fully mature	Description	Usage
p	0.2	0.02	Plasticity rate	Scales α, β, R^+, R^-
r	1.5	1	Excitability of GCs	Equations 2, 7
G_0	0.5 (enriched), 0 (unenriched)	-0.45	Survival threshold	Equation 12

Table 1. Age dependent parameters. GCs were considered immature if they were added to the network within 14 time steps, corresponding to their critical period.

of noise is inversely related to the memory of the network. More significantly, for low levels of noise, the dendritic elaboration was dominated by MC activity, such that GCs predominantly connected to MCs driven by the enrichment even if the spine dynamics were independent of activity. Such specificity in the dendritic network may be unlikely, so we chose a level of noise that allows the memory to decay to zero. This parameter also influences relearning (Figure SI7H). In the range we explored, relearning remained faster than the initial learning on average, but the degree to which relearning was faster was much larger in trials with less noise. Likewise, the size of the dendritic network also affects relearning (Figure SI7I). When we doubled the size of this network, GCs did not need the sensory-dependent dendritic elaboration to learn the odors (Figure 3B), and thus did not leverage the advantage this mechanism provides unless the amount of noise was low. In this scenario however, abGCs that had already fully developed their dendrites at the onset of enrichment were responsible for learning, inconsistent with experiments ***Forest et al.*** (***2019***, 2020) and the results of Figure 3C.

The final parameters we tested were involved in the synaptic plasticity rule. First we looked at the relative rate of consolidation to deconsolidation. Within the range we tested, we saw no significant change in learning ability (Figure SI7E), suggesting that this parameter does not substantially affect any of the results. Finally we tested the parameter k in the sliding threshold $\theta_j^{\pm}$. Compared to other parameters shown, small changes in k resulted in more significant changes. If k was too small, GCs did not prune synapses that were not beneficial to processing the odors, leading to non-specific connectivity and poor learning (Figure SI7F). Alternatively, if k was too large, neurons started to have difficulty consolidating beneficial synapses, also harming learning.

Acknowledgments

This work was supported by the NSF (DMS-1547394) and NIH (DC015137). B.S. was supported by a John N. Nicholson fellowship.

References

Adams W, Graham JN, Han X, Riecke H. Top-down inputs drive neuronal network rewiring and context-enhanced sensory processing in olfaction. PLoS Comp Biology. 2019; 15:e1006611. doi: https://doi.org/10.1101/271197.

Adlaf EW, Vaden RJ, Niver AJ, Manuel AF, Onyilo VC, Araujo MT, Dieni CV, Vo HT, King GD, Wadiche JI, et al. Adult-born neurons modify excitatory synaptic transmission to existing neurons. Elife. 2017; 6:e19886.

Aimone JB. Computational modeling of adult neurogenesis. Cold Spring Harbor Perspectives in Biology. 2016; 8(4):a018960.

Aimone JB, Deng W, Gage FH. Resolving new memories: a critical look at the dentate gyrus, adult neurogenesis, and pattern separation. Neuron. 2011 May; 70(4):589–596.

Aimone JB, Gage FH. Modeling new neuron function: a history of using computational neuroscience to study adult neurogenesis. Eur J Neurosci. 2011 Mar; 33(6):1160–1169.

Aimone JB, Wiles J, Gage FH. Computational Influence of Adult Neurogenesis on Memory Encoding. Neuron. 2009 Jan; 61(2):187–202.

	Value	Description	Usage
N_{MC}	225	Number of MCs	Network architecture
N_{GC}	900	Initial number of GCs	Network architecture
N_{add}	8	Number of GCs added each neurogenesis step	Network architecture
N_{conn}	30	Number of MCs with which a GC can form synapses	Network architecture
N_{init}	10	Number initial synapses made by each abGC	Network architecture
α	1.5	Rate of unconsolidated spine formation	Network architecture
β	1.5	Rate of unconsolidated spine removal	Network architecture
$S^{spontaneous}$	0.1	Spontaneous activity of sensory input	Equation 1
γ	0.004	Inhibitory strength of GCs	Equation 1
θ^M	0.15	Threshold to induce dendritic growth	Equation 4
$\epsilon_{i,j}$	$\sim U(0, 1.3)$	Noise in dendritic formation	Equation 4
R_0	0.01	Spontaneous rate of synaptic changes	Equations 5, 6
g	13	Scaler	Equations 5, 6
d	0.7	Relative rate of deconsolidation to consolidation	Equation 6
C_{pre}	3.6	Presynaptic calcium contribution	Equation 7
C_{post}	1.1	Postsynaptic calcium contribution	Equation 7
τ	3.33	Timescale of calcium dynamics	Equation 7
k	0.95	Consolidation threshold scalar	Equations 10, 11
θ^+	1.05	Minimum threshold for consolidation	Equation 10
θ^-	1	Minimum threshold for deconsolidation	Equation 11

Table 2. Age independent parameters. Parameter values used in the simulation of the model unless stated otherwise.

Akers KG, Martinez-Canabal A, Restivo L, Yiu AP, De Cristofaro A, Hsiang HLL, Wheeler AL, Guskjolen A, Niibori Y, Shoji H, Ohira K, Richards BA, Miyakawa T, Josselyn SA, Frankland PW. Hippocampal Neurogenesis Regulates Forgetting During Adulthood and Infancy. Science. 2014 MAY 9; 344(6184):598–602. doi: 10.1126/science.1248903.

Amit DJ, Fusi S. Learning in neural networks with material synapses. Neural Computation. 1994; 6(5):957–982.

Artola A, Bröcher S, Singer W. Different voltage-dependent thresholds for inducing long-term depression and long-term potentiation in slices of rat visual cortex. Nature. 1990; 347(6288):69–72.

Artola A, Singer W. Long-term depression of excitatory synaptic transmission and its relationship to long-term potentiation. Trends in Neurosciences. 1993; 16(11):480–487.

Benna MK, Fusi S. Computational principles of synaptic memory consolidation. Nature Neuroscience. 2016 Dec; 19:1697–1706. doi: 10.1038/nn.4401.

Benson TE, Ryugo DK, Hinds JW. Effects of sensory deprivation on the developing mouse olfactory system: a light and electron microscopic, morphometric analysis. J Neurosci. 1984 Mar; 4(3):638–653.

Bolding KA, Franks KM. Complementary codes for odor identity and intensity in olfactory cortex. eLife. 2017 Apr; 6. doi: 10.7554/eLife.22630.

Breton-Provencher V, Bakhshetyan K, Hardy D, Bammann RR, Cavarretta F, Snapyan M, Cote D, Migliore M, Saghatelyan A. Principal cell activity induces spine relocation of adult-born interneurons in the olfactory bulb. Nature Communications. 2016 Aug; 7:12659. doi: 10.1038/ncomms12659.

Breton-Provencher V, Cote D, Saghatelyan A. Activity of the principal cells of the olfactory bulb promotes a structural dynamic on the distal dendrites of immature adult-born granule cells via activation of NMDA receptors. Journal of Neuroscience. 2014 Jan; 34:1748–1759. doi: 10.1523/JNEUROSCI.3013-13.2014.

Carleton A, Petreanu LT, Lansford R, Alvarez-Buylla A, Lledo PM. Becoming a New Neuron in the Adult Olfactory Bulb. Nature Neuroscience. 2003 May; 6(5):507–518.

Chow SF, Wick SD, Riecke H. Neurogenesis Drives Stimulus Decorrelation in a Model of the Olfactory Bulb. PLoS Comp Biol. 2012; 8:e1002398.

Christian KM, Song H, Ming Gl. Functions and dysfunctions of adult hippocampal neurogenesis. Annual Review of Neuroscience. 2014; 37:243–262.

Cleland TA, Sethupathy P. Non-Topographical Contrast Enhancement in the Olfactory Bulb. BMC Neurosci. 2006 January; 7:7.

Dahlen JE, Jimenez DA, Gerkin RC, Urban NN. Morphological analysis of activity-reduced adult-born neurons in the mouse olfactory bulb. Front Neurosci. 2011 May; 5:66.

Ebbinghaus H. Über das gedächtnis: Untersuchungen zur experimentellen psychologie. Duncker & Humblot; 1885.

Epp JR, Silva Mera R, Köhler S, Josselyn SA, Frankland PW. Neurogenesis-mediated forgetting minimizes proactive interference. Nature Communications. 2016; 7(1):10838.

Forest J, Chalençon L, Midroit M, Terrier C, Caillé I, Sacquet J, Benetollo C, Martin K, Richard M, Didier A, Mandairon N. Role of Adult-Born Versus Preexisting Neurons Born at P0 in Olfactory Perception in a Complex Olfactory Environment in Mice. Cerebral Cortex. 2020 Mar; 30:534–549.

Forest J, Moreno M, Cavelius M, Chalencon L, Ziessel A, Sacquet J, Richard M, Didier A, Mandairon N. Short-term availability of adult-born neurons for memory encoding. Nature Communications. 2019 Dec; 10:5609. doi: 10.1038/s41467-019-13521-7.

Fusi S, Abbott LF. Limits on the Memory Storage Capacity of Bounded Synapses. Nature Neuroscience. 2007 April; 10(4):485–493.

Fusi S, Drew PJ, Abbott LF. Cascade models of synaptically stored memories. Neuron. 2005 Feb; 45(4):599–611.

Fusi S. Memory capacity of neural network models. arXiv preprint arXiv:210807839. 2021; .

Gao A, Xia F, Guskjolen AJ, Ramsaran AI, Santoro A, Josselyn SA, Frankland PW. Elevation of hippocampal neurogenesis induces a temporally graded pattern of forgetting of contextual fear memories. Journal of Neuroscience. 2018; 38(13):3190–3198.

Gao Y, Strowbridge BW. Long-term plasticity of excitatory inputs to granule cells in the rat olfactory bulb. Nature Neuroscience. 2009 Jun; 12(6):731–733.

Graupner M, Brunel N. Calcium-based plasticity model explains sensitivity of synaptic changes to spike pattern, rate, and dendritic location. Proceedings of the National Academy of Sciences of the United States of America. 2012 Mar; 109(10):3991–3996.

Greco-Vuilloud J, Midroit M, Terrier C, Forest J, Sacquet J, Mandairon N, Didier A, Richard M. 12 months is a pivotal age for olfactory perceptual learning and its underlying neuronal plasticity in aging mice. Neurobiology of Aging. 2022; https://www.sciencedirect.com/science/article/pii/S0197458022000458, doi: https://doi.org/10.1016/j.neurobiolaging.2022.03.003.

Grossberg S. Processing of expected and unexpected events udring conditionand and attention - A psychological theory. Psychological Review. 1982; 89(5):529–572. doi: 10.1037/0033-295X.89.5.529.

Gschwend O, Abraham NM, Lagier S, Begnaud F, Rodriguez I, Carleton A. Neuronal pattern separation in the olfactory bulb improves odor discrimination learning. Nature Neuroscience. 2015 Oct; 18:1474–1482. doi: 10.1038/nn.4089.

Guskjolen A, Cembrowski MS. Engram neurons: Encoding, consolidation, retrieval, and forgetting of memory. Molecular Psychiatry. 2023; 28(8):3207–3219.

Guskjolen A, Dhaliwal J, de la Parra J, Epp JR, Ko S, Chahley E, de Snoo M, Solari M, Panesar P, Snyder JS, et al. Neurogenesis-mediated circuit remodeling reduces engram reinstatement and promotes forgetting. bioRxiv 20231010561722. 2023; .

Hartline HK, Ratliff F. Inhibitory Interaction of Receptor Units in the Eye of Limulus. J Gen Physiol. 1957; 40(3):357–376.

Huszár R, Zhang Y, Blockus H, Buzsáki G. Preconfigured dynamics in the hippocampus are guided by embryonic birthdate and rate of neurogenesis. Nature Neuroscience. 2022; 25(9):1201–1212.

Johnson EM, Kath WL, Mani M. EMBEDR: Distinguishing signal from noise in single-cell omics data. Patterns. 2022; 3(3):100443. https://www.sciencedirect.com/science/article/pii/S2666389922000162, doi: 10.1016/j.patter.2022.100443.

Kaplan MS, Mcnelly NA, Hinds JW. Population-Dynamics of Adult-Formed Granule Neurons of the Rat Olfactory-Bulb. J Compar Neurol. 1985 December; 239(1):117–125.

Kasai H, Ziv NE, Okazaki H, Yagishita S, Toyoizumi T. Spine dynamics in the brain, mental disorders and artificial neural networks. Nature Reviews Neuroscience. 2021 May; 22:407.

Kelsch W, Lin CW, Lois C. Sequential development of synapses in dendritic domains during adult neurogenesis. Proc Natl Acad Sci U S A. 2008 Oct; 105(43):16803–16808.

Kelsch W, Lin CW, Mosley CP, Lois C. A critical period for activity-dependent synaptic development during olfactory bulb adult neurogenesis. J Neurosci. 2009 Sep; 29(38):11852–11858.

Kempermann G, Song H, Gage FH. Neurogenesis in the adult hippocampus. Cold Spring Harbor Perspectives in Biology. 2015; 7(9):a018812.

Kersen DEC, Tavoni G, Balasubramanian V. Connectivity and dynamics in the olfactory bulb. PLoS Computational Biology. 2022 Feb; 18:e1009856.

Komano-Inoue S, Manabe H, Ota M, Kusumoto-Yoshida I, Yokoyama TK, Mori K, Yamaguchi M. Top-down inputs from the olfactory cortex in the postprandial period promote elimination of granule cells in the olfactory bulb. Eur J Neurosci. 2014 Sep; 40(5):2724–2733. http://dx.doi.org/10.1111/ejn.12679, doi: 10.1111/ejn.12679.

Koulakov AA, Kolterman BE, Enikolopov AG, Rinberg D. In search of the structure of human olfactory space. Front Syst Neurosci. 2011; 5:65.

Kudithipudi D, Aguilar-Simon M, Babb J, Bazhenov M, Blackiston D, Bongard J, Brna AP, Chakravarthi Raja S, Cheney N, Clune J, Daram A, Fusi S, Helfer P, Kay L, Ketz N, Kira Z, Kolouri S, Krichmar JL, Kriegman S, Levin M, et al. Biological underpinnings for lifelong learning machines. Nature Machine Intelligence. 2022; 4(3):196–210. https://doi.org/10.1038/s42256-022-00452-0, doi: 10.1038/s42256-022-00452-0.

Li WL, Chu MW, Wu A, Suzuki Y, Imayoshi I, Komiyama T. Adult-born neurons facilitate olfactory bulb pattern separation during task engagement. eLife. 2018 Mar; 7. doi: 10.7554/eLife.33006.

Lin CW, Sim S, Ainsworth A, Okada M, Kelsch W, Lois C. Genetically increased cell-intrinsic excitability enhances neuronal integration into adult brain circuits. Neuron. 2010; 65:32–9.

Livneh Y, Mizrahi A. Experience-dependent plasticity of mature adult-born neurons. Nature Neuroscience. 2012 Nov; 15(1):26–28.

Lledo PM, Alonso M, Grubb MS. Adult Neurogenesis and Functional Plasticity in Neuronal Circuits. Nature Reviews Neuroscience. 2006 March; 7(3):179–193.

Mandairon N, Kermen F, Charpentier C, Sacquet J, Linster C, Didier A. Context-driven activation of odor representations in the absence of olfactory stimuli in the olfactory bulb and piriform cortex. Front Behav Neurosci. 2014; 8:138. http://dx.doi.org/10.3389/fnbeh.2014.00138, doi: 10.3389/fnbeh.2014.00138.

McClelland JL, McNaughton BL, O'Reilly RC. Why there are complementary learning systems in the hippocampus and neocortex: insights from the successes and failures of connectionist models of learning and memory. Psychological Review. 1995; 102(3):419.

McNamara AM, Magidson PD, Linster C, Wilson DA, Cleland TA. Distinct Neural Mechanisms Mediate Olfactory Memory Formation At Different Timescales. Learning & Memory. 2008 March; 15(3):117–125.

Meltzer LA, Yabaluri R, Deisseroth K. A Role for Circuit Homeostasis in Adult Neurogenesis. Trends Neurosci. 2005 December; 28(12):653–660.

Meng JH, Riecke H. Structural spine plasticity: Learning and forgetting of odor-specific subnetworks in the olfactory bulb. PLOS Computational Biology. 2022 10; 18(10):1–30. https://doi.org/10.1371/journal.pcbi.1010338, doi: 10.1371/journal.pcbi.1010338.

Mizrahi A. Dendritic development and plasticity of adult-born neurons in the mouse olfactory bulb. Nature Neuroscience. 2007 Apr; 10(4):444–452.

Moreno MM, Linster C, Escanilla O, Sacquet J, Didier A, Mandairon N. Olfactory perceptual learning requires adult neurogenesis. Proc Natl Acad Sci U S A. 2009 Oct; 106(42):17980.

Mouret A, Gheusi G, Gabellec MM, de Chaumont F, Olivo-Marin JC, Lledo PM. Learning and survival of newly generated neurons: when time matters. J Neurosci. 2008 Nov; 28(45):11511–11516.

Mouret A, Lepousez G, Gras J, Gabellec MM, Lledo PM. Turnover of newborn olfactory bulb neurons optimizes olfaction. J Neurosci. 2009 Sep; 29(39):12302–12314.

Nissant A, Bardy C, Katagiri H, Murray K, Lledo PM. Adult neurogenesis promotes synaptic plasticity in the olfactory bulb. Nature Neuroscience. 2009 Jun; 12(6):728–730.

Park DK, Petshow S, Anisimova M, Barragan EV, Gray JA, Stein IS, Zito K. Reduced d-serine levels drive enhanced non-ionotropic NMDA receptor signaling and destabilization of dendritic spines in a mouse model for studying schizophrenia. Neurobiology of Disease. 2022; 170:105772.

Pedregosa F, Varoquaux G, Gramfort A, Michel V, Thirion B, Grisel O, Blondel M, Prettenhofer P, Weiss R, Dubourg V, Vanderplas J, Passos A, Cournapeau D, Brucher M, Perrot M, Duchesnay E. Scikit-learn: Machine Learning in Python. Journal of Machine Learning Research. 2011; 12:2825–2830.

Platel JC, Angelova A, Bugeon S, Wallace J, Ganay T, Chudotvorova I, Deloulme JC, Beclin C, Tiveron MC, Core N, Murthy VN, Cremer H. Neuronal integration in the adult mouse olfactory bulb is a non-selective addition process. eLife. 2019 jul; 8:e44830. https://doi.org/10.7554/eLife.44830, doi: 10.7554/eLife.44830.

Rochefort C, Gheusi G, Vincent JD, Lledo PM. Enriched Odor Exposure Increases the Number of Newborn Neurons in the Adult Olfactory Bulb and Improves Odor Memory. J Neurosci. 2002 April; 22(7):2679–2689.

Roxin A, Fusi S. Efficient partitioning of memory systems and its importance for memory consolidation. PLoS Comput Biol. 2013 Jul; 9(7):e1003146. http://dx.doi.org/10.1371/journal.pcbi.1003146, doi: 10.1371/journal.pcbi.1003146.

Saghatelyan A, Roux P, Migliore M, Rochefort C, Desmaisons D, Charneau P, Shepherd GM, Lledo PM. Activity-dependent adjustments of the inhibitory network in the olfactory bulb following early postnatal deprivation. Neuron. 2005 Apr; 46(1):103–116.

Saha S, Meng JH, Riecke H, Agoranos G, Sailor KA, Lledo PM. Interneuron activity-structural plasticity association is driven by context-dependent odor experience. bioRxiv 20210128428612. 2021; .

Sailor KA, Valley MT, Wiechert MT, Riecke H, Sun GJ, Adams W, Dennis JC, Sharafi S, Ming GL, Song H, Lledo PM. Persistent Structural Plasticity Optimizes Sensory Information Processing in the Olfactory Bulb. Neuron. 2016 Jul; 91(2):384–396. http://dx.doi.org/10.1016/j.neuron.2016.06.004, doi: 10.1016/j.neuron.2016.06.004.

Shani-Narkiss H, Vinograd A, Landau ID, Tasaka G, Yayon N, Terletsky S, Groysman M, Maor I, Sompolinsky H, Mizrahi A. Young adult-born neurons improve odor coding by mitral cells. Nature Communications. 2020 Nov; 11:5867.

Soucy ER, Albeanu DF, Fantana AL, Murthy VN, Meister M. Precision and diversity in an odor map on the olfactory bulb. Nature Neuroscience. 2009 Feb; 12(2):210–220.

Stein IS, Park DK, Claiborne N, Zito K. Non-ionotropic NMDA receptor signaling gates bidirectional structural plasticity of dendritic spines. Cell Reports. 2021; 34(4):108664. https://www.sciencedirect.com/science/article/pii/S2211124720316533, doi: 10.1016/j.celrep.2020.108664.

Sultan S, Mandairon N, Kermen F, Garcia S, Sacquet J, Didier A. Learning-Dependent Neurogenesis in the Olfactory Bulb Determines Long-Term Olfactory Memory. Faseb J. 2010 July; 24(7):2355–2363.

Sultan S, Lefort JM, Sacquet J, Mandairon N, Didier A. Acquisition of an olfactory associative task triggers a regionalized down-regulation of adult born neuron cell death. Front Neurosci. 2011 May; 5:52.

Terrier C, Greco-Vuilloud J, Cavelius M, Thevenet M, Mandairon N, Didier A, Richard M. long-term olfactory enrichment promotes non-olfactory cognition, noradrenergic plasticity and remodeling of brain functional connectivity in older mice. Neurobiology of Aging. 2024; .

The MathWorks Inc , Optimization Toolbox version: 9.4 (R2022b). Natick, Massachusetts, United States: The MathWorks Inc.; 2022. https://www.mathworks.com.

Tran LM, Josselyn SA, Richards BA, Frankland PW. Forgetting at biologically realistic levels of neurogenesis in a large-scale hippocampal model. Behavioural Brain Research. 2019; 376:112180.

Vardalaki D, Chung K, Harnett MT. Filopodia are a structural substrate for silent synapses in adult neocortex. Nature. 2022; 612(7939):323–327. https://doi.org/10.1038/s41586-022-05483-6, doi: 10.1038/s41586-022-05483-6.

Veyrac A, Sacquet J, Nguyen V, Marien M, Jourdan F, Didier A. Novelty determines the effects of olfactory enrichment on memory and neurogenesis through noradrenergic mechanisms. Neuropsychopharmacology. 2009 Feb; 34(3):786–795.

Wallace JL, Wienisch M, Murthy VN. Development and Refinement of Functional Properties of Adult-Born Neurons. Neuron. 2017; http://dx.doi.org/10.1016/j.neuron.2017.09.039, doi: 10.1016/j.neuron.2017.09.039.

Wick S, Wiechert M, Friedrich R, Riecke H. Pattern orthogonalization via channel decorrelation by adaptive networks. J Comput Neurosci. 2010 Aug; 28:29–45.

Wiechert MT, Judkewitz B, Riecke H, Friedrich RW. Mechanisms of pattern decorrelation by recurrent neuronal circuits. Nature Neuroscience. 2010 Aug; 13(8):1003–1010.

Wilson CD, Serrano GO, Koulakov AA, Rinberg D. A primacy code for odor identity. Nature Communications. 2017 Nov; 8:1477. doi: 10.1038/s41467-017-01432-4.

Wong ROL, Ghosh A. Activity-dependent regulation of dendritic growth and patterning. Nature Reviews Neuroscience. 2002; 3:803–812. doi: 10.1038/nrn941.

Yamaguchi M, Manabe H, Murata K, Mori K. Reorganization of neuronal circuits of the central olfactory system during postprandial sleep. Front Neural Circuits. 2013; 7:132. http://dx.doi.org/10.3389/fncir.2013.00132, doi: 10.3389/fncir.2013.00132.

Yamaguchi M, Mori K. Critical period for sensory experience-dependent survival of newly generated granule cells in the adult mouse olfactory bulb. Proc Natl Acad Sci U S A. 2005 Jul; 102(27):9697–9702.

Yokoyama TK, Mochimaru D, Murata K, Manabe H, Kobayakawa K, Kobayakawa R, Sakano H, Mori K, Yamaguchi M. Elimination of Adult-Born Neurons in the Olfactory Bulb Is Promoted during the Postprandial Period. Neuron. 2011 Sep; 71(5):883–897.

Yoshihara Si, Takahashi H, Nishimura N, Naritsuka H, Shirao T, Hirai H, Yoshihara Y, Mori K, Stern PL, Tsuboi A. 5T4 glycoprotein regulates the sensory input-dependent development of a specific subtype of newborn interneurons in the mouse olfactory bulb. Journal of Neuroscience. 2012; 32(6):2217–2226.

Yoshihara Si, Takahashi H, Tsuboi A. Molecular Mechanisms Regulating the Dendritic Development of Newborn Olfactory Bulb Interneurons in a Sensory Experience-Dependent Manner. Frontiers in Neuroscience. 2016 JAN 12; 9. doi: 10.3389/fnins.2015.00514.

Supplementary information

Discriminability

In addition to using a connectivity-based learning measure, we use an activity-based learning measure to characterize to what extent learning enhances the ability of downstream cortical neurons to discriminate between the odors based on their read-out of the MC activities. Because the MC rate model does not include any fluctuations in activity that would limit discriminability, we assume that the rates represent the mean values of independent Poisson spike trains for which the variance is given by their mean. We assume a linear read-out of the MC activities with the weights chosen optimally and characterize the discriminability of stimuli A and B in terms of the optimal Fisher discriminant F_{opt} ***Adams et al.*** (***2019***),

$$F_{opt} = \sum_{i=1}^{N_{MC}} \frac{(M_i^{(A)} - M_i^{(B)})^2}{M_i^{(A)} + M_i^{(B)}}. \tag{1}$$

Thus, it can be seen that F_{opt} will increase with the addition of MCs, reflecting the fact that even poorly discriminating MCs provide some additional information about the odors.

To verify that our connectivity-based measure of memory aligns with the function of the OB, we calculated the time course of the Fisher discriminant using the data that generated the results in Figure 2C (Figure S1B). Indeed, both measures yield qualitatively similar results, with the fast network learning and forgetting quickly, the slow network learning and forgetting slowly, and the age-dependent network learning quickly and forgetting slowly. Likewise, the neurogenic and non-neurogenic networks performed similarly.

In this study, we focused on the changes in the network connectivity rather than changes in MC activity. We therefore assessed the behavior of the system mostly in terms of the connectivity-based memory. This measure for the memory is agnostic with respect to the odor code, i.e. it does not depend on the type of read-out of the OB activity used by the animal (e.g. rate-based or timing-based ***Wilson et al.*** (***2017***); ***Bolding and Franks*** (***2017***)).

Comparison with other methods resolving the flexibility-stability dilemma

Previous theoretical work has established a general framework in order to track the memory of an arbitrary stimulus in a stream of random uncorrelated stimuli based only on the properties of the network, without explicitly modeling neuronal activity. It has been used to evaluate models that confront the flexibility-stability dilemma ***Fusi et al.*** (***2005***); ***Roxin and Fusi*** (***2013***); ***Benna and Fusi*** (***2016***); ***Fusi*** (***2021***). In networks with N simple synapses where plasticity occurs on a uniformly fast time scale, the initial memory grows as $\sqrt{N}$ while overall memory capacity grows only logarithmically with N ***Amit and Fusi*** (***1994***); ***Fusi and Abbott*** (***2007***). Meanwhile, the complex synapses of the cascade model ***Fusi et al.*** (***2005***) and the bidirectional cascade model ***Benna and Fusi*** (***2016***) as well as the heterogeneity and structure of the partitioned memory system model ***Roxin and Fusi*** (***2013***) have been shown to allow the network to achieve far greater capacity. In the case of the cascade model and the partitioned memory system model, memory capacity on the order of $\sqrt{N}$ can be achieved, and in the case of the bidirectional cascade model memory capacity on the order of N can be achieved, though the latter requires a great degree of complexity in the synapses.

To understand the scaling properties of our model and how they compare with other models, we situated it within this framework. More specifically, we consider a network initially with N binary synapses. At each time step, each synapse is independently presented with a plasticity event, which attempts to flip the synapse depending on the presented stimulus and is accepted with probability q_i, the plasticity rate of synapse i (Figure S6A). To quantify memory performance, we tracked the signal-to-noise ratio (SNR) of a single arbitrary stimulus previously encoded by the network (Figure S6B). We report the flexibility as the SNR immediately after stimulus presentation (the "initial memory" SNR(0)). The stability we characterize in terms of the time T that it took for the SNR to decay to the value of 1 due to the storage of subsequent memories (the "memory lifetime"), which can be interpreted as the memory capacity. The presented stimuli are random and uncorrelated. Thus, on average the initial memory signal $\mu_i(t=0)$ of a stimulus associated with synapse i is q_i and the total initial memory signal $\mu(0)$ of the network is

$$\mu(0) = \sum_{i=1}^{N} \mu_i(0) = \sum_{i=1}^{N} q_i. \tag{2}$$

Meanwhile, as this is a system of binomially distributed variables, the variance of the signal can be roughly approximated as $\sqrt{N}$ ***Roxin and Fusi*** (***2013***), leading to a signal-to-noise ratio $SNR(0)$ of

$$SNR(0) = \frac{1}{\sqrt{N}} \sum_{i=1}^{N} q_i. \tag{3}$$

As ***Roxin and Fusi*** (***2013***) show, the dynamics of the signal to noise ratio of the memory can be described by

$$\frac{dSNR}{dt} = \frac{1}{\sqrt{N}} \sum_{i=1}^{N} \frac{d\mu_i}{dt} \tag{4}$$

where the $\mu_i(t)$ follow the equations

$$\frac{d\mu_i}{dt} = -q_i \mu_i. \tag{5}$$

To incorporate the key element of our plasticity model, we extend this model by making the plasticity rates q_i depend on the ages of the cells such that

$$q_i = \begin{cases} q^{fast} & \text{if age of GC } i \text{ is} \leq T_c \text{ days} \\ q^{slow} & \text{if age of GC } i \text{ is} > T_c \text{ days,} \end{cases} \tag{6}$$

where $q^{fast} \gg q^{slow}$ and T_c is the duration of the critical period during which the synapse is highly plastic. Following ***Fusi et al.*** (***2005***), we choose $q^{fast} \sim \mathcal{O}(1)$ and $q^{slow} \sim \mathcal{O}(N^{-\frac{1}{2}})$. If, at the time of the stimulus presentation, the fraction of synapses on young GCs is k, then according to Eq.3 the SNR of that memory is given by

$$SNR(0) = \sqrt{N}(kq^{fast} + (1-k)q^{slow}). \tag{7}$$

If $kq^{fast} \gg q^{slow}$, the initial memory is controlled by the fast plasticity rate, $SNR(0) \sim \sqrt{N}kq^{fast}$. Indeed, in the rat brain the total number of GCs is a few million, while roughly 10,000 more are born on each day ***Kaplan et al.*** (***1985***). Since the critical period lasts about 14 days, about 140,000 GCs have enhanced plasticity, so k is on the order of 0.1. Thus assuming $N \sim 10^8$, $kq^{fast} \approx 10^{-1} \gg q^{slow} \approx 10^{-4}$ is a valid assumption.

The memory duration is determined by the time T at which $SNR(t)$ falls below some fixed threshold θ_{SNR}. Solving Eqs.3-6, we have that for $t \geq T_c$, $SNR(t)$ is given by

$$\begin{aligned} SNR(t) \quad = \quad & \Bigg[q^{slow}(1-k)\sqrt{N} + \\ & q^{fast}\frac{k\sqrt{N}}{T_c}\sum_{j=0}^{T_c} e^{(q^{slow}-q^{fast})j} \Bigg] e^{-q^{slow}t}. \end{aligned} \tag{8}$$

We use this to solve for the memory duration T where $SNR(T) = \theta_{SNR}$. Again, using $q^{slow} \sim \mathcal{O}(\frac{1}{\sqrt{N}})$ and $q^{fast} \sim \mathcal{O}(1)$ we get

$$T = \sqrt{N}\log\left[\frac{1-k}{\theta_{SNR}} + \frac{k\sqrt{N}}{T_c\theta_{SNR}}\sum_{j=0}^{T_c} e^{(\frac{1}{\sqrt{N}}-1)j}\right]. \tag{9}$$

For large N, memory duration scales approximately as $T \sim \mathcal{O}(\sqrt{N}\log(\sqrt{N}))$, where the leading $\sqrt{N}$ arises from the inverse of q^{slow}. This shows that while initial memory is controlled by the fast plasticity of immature synapses, memory duration is controlled by the slow plasticity rate of mature synapses.

We verified these results computationally. First we compared the memory decay of our model to those of homogeneous models as well as the cascade model and the partitioned memory system model for a network of approximate size to the rat OB (Figure S6C). We show our model (red) has a similar initial memory and memory duration as the cascade model (blue) and the partitioned memory system model (green), all of which far outpace the initial memory of the slow-synapse model (grey) and the memory duration of the fast-synapse model (black). Notably, this reiterates that the increased memory capacity provided by neurogenesis is due to the age-dependent properties of adult-born neurons rather than the addition of neurons alone, and that this age-dependence can most efficient utilize the new synapses provided by adult neurogenesis.

Finally, we examine how the initial memory and the memory duration scale with N (Figure S6D). We confirm that both the initial memory (Figure S6E) as well as the memory lifetime approximately follow $\sqrt{N}$ (Figure S6F). Thus, like the cascade model and the partitioned-memory model, our age-dependent model robustly resolves the plasticity-flexibility dilemma, simultaneously achieving the greatest initial memory and memory duration possibly afforded by the homogeneous network with constant plasticity.

Supplementary Figures

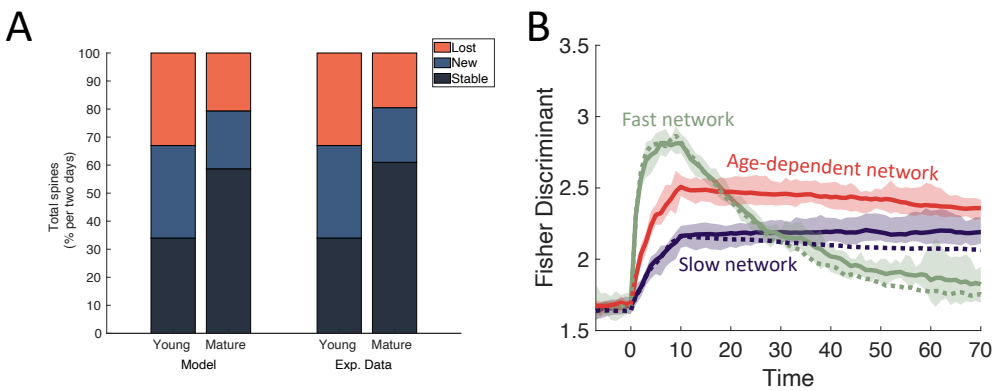

Figure S1. (Related to Figure 2) Spine turnover and consistency of memory measure. (A) Parameters governing spine turnover were fit so that the two day spine turnover rates in young and mature abGCs matched those previously reported in ***Sailor et al.*** (***2016***). (B) Odor-discriminability as characterized by the Fisher discriminant (Supplementary Information “Discriminability") exhibits the same behavior as the connectivity-based memory shown in Figure 2C.

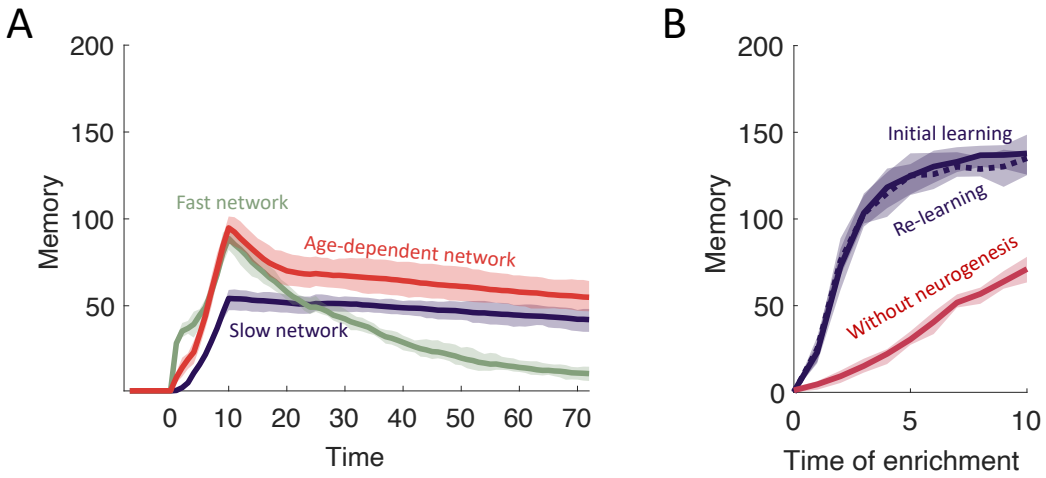

Figure S2. (Related to Figure 3) Dependence of memory on dendritic development (A) The same memory measurements were taken as in Fig.2C for the model with sensory-dependent dendritic development as well as increased excitability. The results are similar to those in Fig.2E, although the shifted birth-date dependence of abGC recruitment (Figure 3C) means that odor-encoding GCs are still in their critical period at the end of enrichment, leading to a short period of rapid memory decay. (B) Repeating the simulation in Figure 3D,F without sensory-dependent dendritic development. Relearning is no longer faster than the initial learning and is especially slow when neurogenesis is blocked. Here, $N_{conn} = 100$ to allow the network to learn fully.

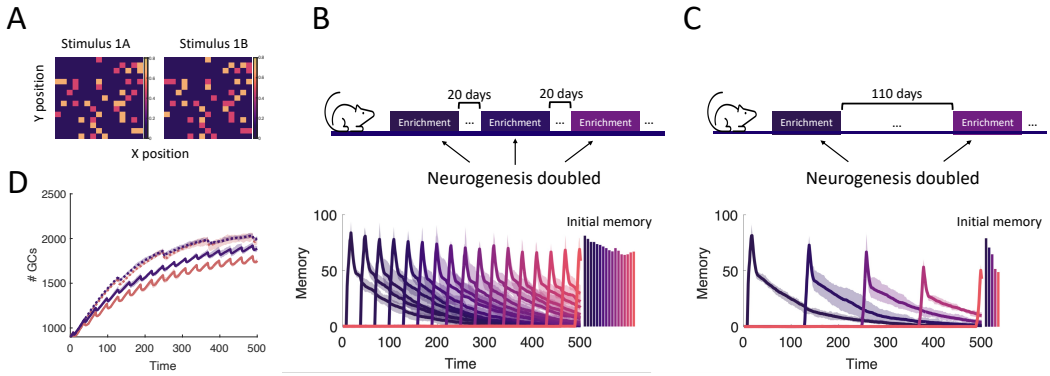

Figure S3. (Related to Figure 4) Effects of increased abGC survival during enrichment. (A) Example sparse, random stimuli. For each stimulus pair, 20% of MCs were randomly selected to be stimulated. Of these MCs, half were highly stimulated and half were moderately stimulated for the first stimulus in the pair. For the second stimulus, the MCs that were previously highly stimulated were moderately stimulated and those that were previously moderately stimulated became highly stimulated. This was to ensure the stimuli in the pair are difficult to discriminate. (B,C) Simulations in Figure 4D,E were repeated while doubling the number of new, fully functional abGCs on each day of enrichment to mimic the established results that olfactory enrichment increases the number of abGCs that survive until they start integrating into the network ***Rochefort et al.*** (***2002***). This functional doubling of neurogenesis slightly increases the initial memory of each enrichment (see also Figure S7D), but does not impact the prediction that more frequent enrichment improves memory. (D) The number of GCs over time for the model with a constant neurogenesis rate (orange) and with enrichment-increased neurogenesis (purple). Solid lines indicate trials with 20 day inter-enrichment intervals (orange: Figure 4D, purple: Figure S3B), dotted lines indicate trials with 110 day inter-enrichment intervals (orange: Figure 4E, purple: Figure S3C).

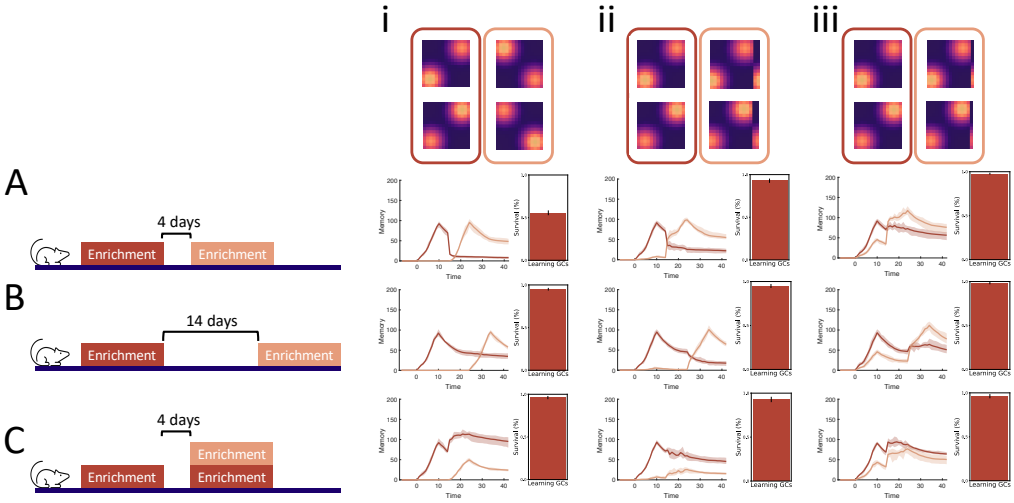

Figure S4. (Related to Figure 4) Retrograde interference The experiments in ***Forest et al.*** (***2019***) were simulated for different pairs of artificial stimuli. (A-C) Experimental protocols in ***Forest et al.*** (***2019***). There were two enrichment periods with two different pairs of stimuli separated by either a 4 (A,C) or 14 (B) day interval. In (C) the odors from the first enrichment were also presented during the second enrichment period in addition to the new odors. (i-iii) Enrichment stimuli. In (i) the enrichment odors were largely non-overlapping. For (ii) and (iii), moderately and highly overlapping stimuli were generated, respectively, by using for stimulus 2 correspondingly cyclically shifted versions of stimulus 1. Line plots show the memory traces resulting from the enrichment protocol marked with the corresponding color in the same row and the stimuli in the same column. Lines: mean over eight trials, shaded areas: range of values. Bar plots show the percentage of GCs that encoded the first enrichment that survived at the end of the simulation. Odor-encoding GCs were determined by clustering the connectivity of GCs at the end of the first enrichment (cf. Fig.2). Bars indicate the mean and error bars show the standard deviation. (Ai) The memory of the first enrichment was extinguished during the second enrichment and there was a significant level of apoptosis among odor-encoding GCs. (Bi) The second enrichment did not substantially affect the initial memory, and there was little apoptosis among odor-encoding GCs. (Ci) The initial memory and the GCs that encoded that memory persist through the second enrichment. (Aii) There is a significant decline in the initial memory during the second enrichment, although the odor-encoding GCs survive throughout the simulation, indicating the memory decline is a result of overwriting rather than apoptosis. (Bii) A slight memory decline occurs during the second enrichment. (Cii) The initial memory is maintained, but the network struggles to encode the second memory. (Aiii-Ciii) The second enrichment does not lead to any deficit in the initial memory, and there is no significant apoptosis.

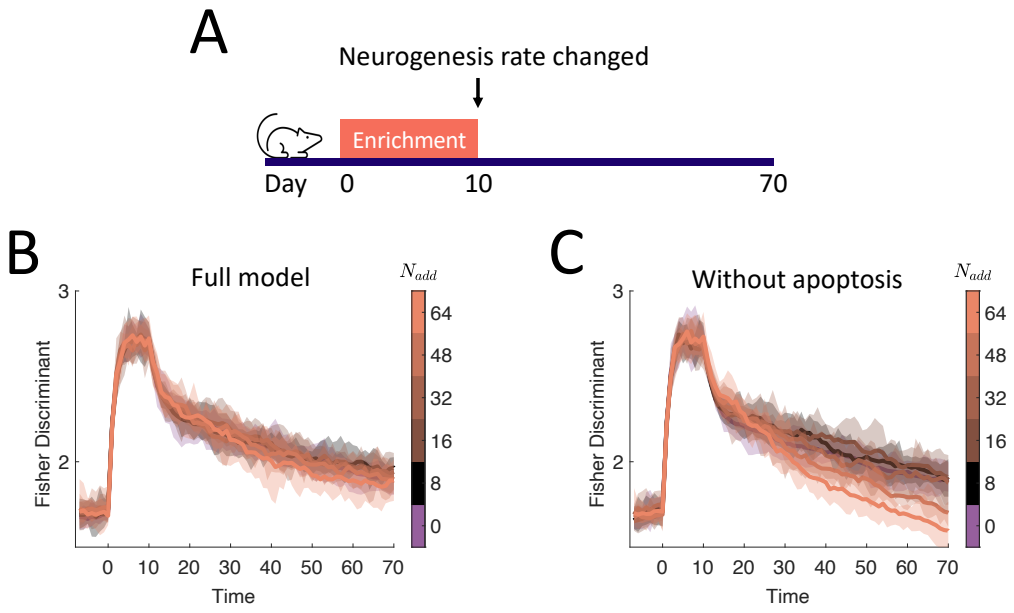

Figure S5. Post-learning changes in neurogenesis rate. (A) Simulation protocol. Following a 10 day enrichment (using the odors in Figure 2B), the neurogenesis rate was permanently changed. (B, C) Fisher discriminant between the two similar odors for the full model and the model without apoptosis. The Fisher discriminant was chosen in order to investigate the degree that abGCs interfere with MC activity, which represents the output of the network. The full model can tolerate the addition of vast numbers of new neurons without substantially affecting memory. Without apoptosis, the accumulation of neurons has substantial impact on memory. Lines: mean values over eight simulations. Shaded area: full range of values.

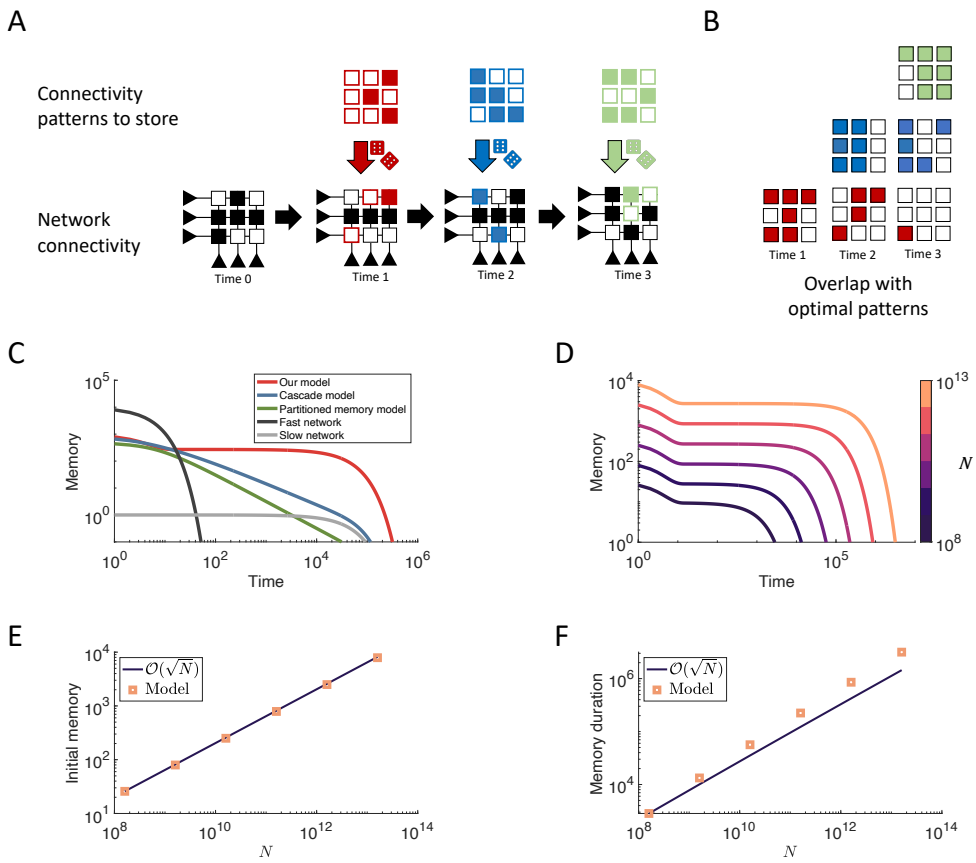

Figure S6. Mean-field model. (A) We assume there exists an optimal configuration that can process a given stimulus. In this framework, the network directly encodes this configuration stochastically according to the plasticity rate at each synapse, and at each time point a new stimulus is presented to the network. We track the memory of the network as the degree of overlap between the optimal network for a given stimulus and the current configuration of the network (see Supplementary Information "Comparison with other methods resolving the flexibility-stability dilemma"). Note that a lack of connection can also represent an overlap. B) Overlap between each stimulus and the current configuration of the network in (A). (C) Results of the mean-field approximation to the model described in (A) with age-dependent synaptic plasticity rates has similar initial memory and memory duration as the cascade model ***Fusi et al.*** (***2005***), and the partitioned-memory model ***Roxin and Fusi*** (***2013***). (D) Results of the age-dependent model for different values of the number of synapses N. (E) Initial memory as a function of N. (F) Memory duration as a function of N.

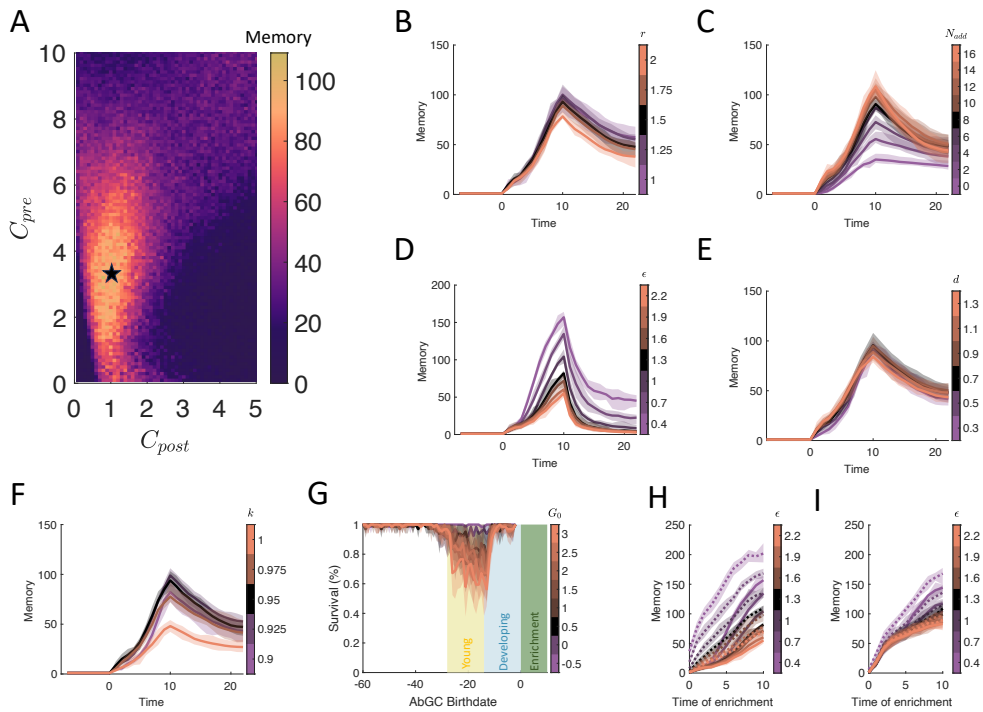

Figure S7. Parameter sensitivity. In all plots the values indicated in black are the parameter values used throughout this study. Lines indicate the mean and shaded areas represent the range over eight trials. (A) Final memory following the standard enrichment experiment as a function of C_{pre} and C_{post}. (B-F) Memory trace over the course of the standard enrichment experiment for different values of r (for abGCs in their critical period), N_{add}, ϵ, d, and k, respectively. In (D), R_0 was increased to 1 following enrichment to illustrate the final memory value after forgetting. (G) GC survival following enrichment for different values of G_0 during the critical period of the abGCs (cf. Figure 4C) (H) Results of the relearning experiment (cf. Figure 3F) for different values of ϵ. Solid: initial learning, dashed: re-learning. (I) As in (H) but for $N_{conn} = 60$ instead of 30.